International Journal of Nanomedicine

Dovepress

open access to scientific and medical research

Open Access Full Text Article

ORIGINAL RESEARCH

Dual Drug-Loaded Coaxial Nanofiber Dressings for the Treatment of Diabetic Foot Ulcer

Dunia A Alzahrani[1], Khulud A Alsulami[1], Fatemah M Alsulaihem[1], Abrar A Bakr[1], Rayan Y Booq[2], Ahmed J Alfahad[3], Alhassan H Aodah[1], Samar A Alsudir[4], Amany A Fathaddin[5,6], Essam J Alyamani[2], Aliyah A Almomen[7], Essam A Tawfik[1]

[1]Advanced Diagnostics and Therapeutics Technologies Institute, Health Sector, King Abdulaziz City for Science and Technology (KACST), Riyadh, 11442, Saudi Arabia; [2]Wellness and Preventative Medicine Institute, Health Sector, King Abdulaziz City for Science and Technology (KACST), Riyadh, 11442, Saudi Arabia; [3]Waste Management and Recycling Technologies Institute, Sustainability and Environment Sector, King Abdulaziz City for Science and Technology (KACST), Riyadh, 11442, Saudi Arabia; [4]Bioengineering Institute, Health Sector, King Abdulaziz City for Science and Technology (KACST), Riyadh, 11442, Saudi Arabia; [5]Department of Pathology, College of Medicine, King Saud University, Riyadh, 12372, Saudi Arabia; [6]King Saud University Medical City, Riyadh, 12372, Saudi Arabia; [7]Department of Pharmaceutical Chemistry, College of Pharmacy, King Saud University, Riyadh, 11451, Saudi Arabia

Correspondence: Essam A Tawfik, Email etawfik@kacst.gov.sa

Introduction: Diabetes mellitus is frequently associated with foot ulcers, which pose significant health risks and complications. Impaired wound healing in diabetic patients is attributed to multiple factors, including hyperglycemia, neuropathy, chronic inflammation, oxidative damage, and decreased vascularization.

Rationale: To address these challenges, this project aims to develop bioactive, fast-dissolving nanofiber dressings composed of polyvinylpyrrolidone loaded with a combination of an antibiotic (moxifloxacin or fusidic acid) and anti-inflammatory drug (pirfenidone) using electrospinning technique to prevent the bacterial growth, reduce inflammation, and expedite wound healing in diabetic wounds.

Results: The fabricated drug-loaded fibers exhibited diameters of 443 ± 67 nm for moxifloxacin/pirfenidone nanofibers and 488 ± 92 nm for fusidic acid/pirfenidone nanofibers. The encapsulation efficiency, drug loading and drug release studies for the moxifloxacin/pirfenidone nanofibers were found to be 70 ± 3% and 20 ± 1 μg/mg, respectively, for moxifloxacin, and 96 ± 6% and 28 ± 2 μg/mg, respectively, for pirfenidone, with a complete release of both drugs within 24 hours, whereas the fusidic acid/pirfenidone nanofibers were found to be 95 ± 6% and 28 ± 2 μg/mg, respectively, for fusidic acid and 102 ± 5% and 30 ± 2 μg/mg, respectively, for pirfenidone, with a release rate of 66% for fusidic acid and 80%, for pirfenidone after 24 hours. The efficacy of the prepared nanofiber formulations in accelerating wound healing was evaluated using an induced diabetic rat model. All tested formulations showed an earlier complete closure of the wound compared to the controls, which was also supported by the histopathological assessment. Notably, the combination of fusidic acid and pirfenidone nanofibers demonstrated wound healing acceleration on day 8, earlier than all tested groups.

Conclusion: These findings highlight the potential of the drug-loaded nanofibrous system as a promising medicated wound dressing for diabetic foot applications.

Keywords: diabetes mellitus, diabetic foot ulcers, nanofibers, electrospinning, drug delivery, wound healing, moxifloxacin, fusidic acid, pirfenidone

Introduction

Diabetic foot ulcer (DFU) is a slow-healing open wound or sore and a common complication associated with diabetes.[1] There are several pathological changes associated with diabetes that impair most of the wound healing processes including several intrinsic factors such as peripheral neuropathy, vascular problems and other complications, as well as extrinsic factors such as wound infection, callus formation and excessive pressure on the site.[2–4] Untreated diabetic foot ulcers often become a source of infection, delaying wound healing and causing severe pain to the patient. This can result in hospitalization and amputation of the lower extremities.[5] The most frequently isolated microorganism in the infected diabetic wound is an aerobic Gram-positive

Received: 7 March 2024
Accepted: 21 May 2024
Published: 11 June 2024

bacterium, *Staphylococcus aureus* (*S. aureus*). Streptococci, Enterococci, Enterobacteriaceae, and Pseudomonas are also common bacteria found in diabetic foot infections (DFI).[6,7]

Standard treatment involves cleansing the ulcer with saline every week, debriding or removing inactive tissue with a surgical blade to facilitate cell proliferation, and covering it with sterile gauze to keep it moist and to reduce the risk of infection and promote healing of the wound.[8–10] Infections are treated with either systematic antibiotics, topical antibiotics, or a combination of the two, depending on the severity and type of infection.[11] DFU wounds need dressing materials capable of promoting healing and isolating the wound site from pathogen microbes. An ideal wound dressing must be in close contact with the wound, absorb the exudates produced by the wound, protect against bacterial invasion, facilitate substance exchange, have exceptional mechanical performance, have a high porosity and swelling capacity, possibility of delivering bioactive agents and maintain the optimum moist environment to promote the healing process.[12–16]

As a wound dressing for DFU, a variety of natural and synthetic polymers have been utilized, including hydrocolloids, hydrogels, foams, and electrospun nanofibers.[15,17] Among the distinctive features of electrospinning-based nanofiber dressings are the ability to be synthesized with different pore sizes which prevent microorganisms from invading, create an ideal moisture environment, can encapsulate or adsorb multiple bioactive molecules such as drugs and growth factors and have a large surface area, which is favorable for drug loading and sustained delivery.[18,19] Moreover, nanofibers mimic the extracellular matrix in their porous structure, which encourages cell attachment and proliferation.[20–22] Electrospun nanofibers have been fabricated and applied as wound dressing from a variety of natural polymers including chitosan, gelatin, collagen, and silk, as well as, synthetic polymers such as polycaprolactone, polyurethane, polyvinyl pyrrolidone (PVP), and polyvinyl alcohol (PVA).[23] PVP is an FDA-approved hydrophilic polymer with easy spinnability, high porosity, biocompatibility and biodegradability, which makes it suitable for a wide variety of pharmaceutical and biomedical uses, including wound dressings.[24–26] In addition, this polymer has a mucoadhesive property, making it suitable for use in biomedical applications and drug delivery systems. The large surface-to-volume ratio and ultrafast disintegration of the PVP nanofibers allow this fibrous system for the immediate release of the encapsulated drugs, making them particularly useful in drug delivery systems.[27,28] It has been reported previously that nanofibers prepared from PVP exhibit a good mechanical property, which was measured as elongation at break (%), and ultimate tensile strength as 9.10 ± 0.2% and 2.30 ± 0.2 Mpa, respectively.[29]

Recently, the use of modified electrospun nanofiber strategies has gained attention in various biomedical applications, including skin wound healing. Zhang et al designed an innovative electrospun nanofiber that combined the properties of nanofibers with the high wound exudate-absorbing ability and moist healing-promoting environment of a hydrogel.[30] Specifically, they developed a Polyasparthydrazide (PAHy) nanofibrous/nanoparticle hydrogel dressing containing 0.5 wt % silver nitrate (AgNO3). This combination has demonstrated antibacterial and wound healing-promoting capacities in a full-thickness wound model. Another recent study has shown the effectiveness of a modified electrospinning strategy that combined the strong mechanical properties of electrospun nanoyarn-woven textiles with nanofiber properties loaded with Chinese herbal extracts.[31] This approach accelerated wound closure, enhanced collagen deposition, improved re-epithelialization and neovascularization, and increased hair follicle formation in a streptozotocin-induced diabetic mouse model with full-thickness skin wounds. These findings highlight the potential of using modified electrospun nanofiber strategies to develop advanced wound dressings with additive properties, such as improved exudate management, promotion of a moist healing environment, antibacterial activity, and enhanced wound healing outcomes.

Moxifloxacin (Moxi) is a broad-spectrum antibiotic effective against a variety of Gram-positive bacteria such as *S. aureus*. Since Moxi has broad antibacterial properties, high efficiency, and can promote wound healing in infected wounds, it is an ideal candidate for wound therapy.[32–34] Fusidic acid (Fus) is another antibiotic that is available in different formulations including cream, ointments and gel and is widely used topically to treat skin infections.[11,35] Pirfenidone (Pir), an FDA-approved therapeutic drug primarily used for idiopathic pulmonary fibrosis, has demonstrated various beneficial properties for potential wound healing treatments. It exhibits anti-inflammatory, antioxidative, and anti-scarring activities, as supported by previous studies.[36–41] Notably, Pir has been shown to effectively reduce tissue inflammation by decreasing pro-inflammatory cytokines, chemokines, neutrophil infiltration, and collagen deposition within wounds. Additionally, it has been found to mitigate the generation of reactive oxygen species (ROS) in separate investigations.[38]

For the bioactive dressing, various types of drugs, such as antibiotics, growth factors, anti-inflammatories and anesthetics, have been delivered using nanofiber systems to enhance the treatment of chronic wound infections, prevent scarring, and enhance wound healing.[11,42–45] For instance, cephradine-loaded gelatin/PVA nanofiber has been reported for its antibacterial activity against *S. aureus* in an induced chronic wound.[46] Iqbal et al have developed chitosan (CS)/PVA nanofibers loaded with the broad-spectrum antibiotic cefadroxil monohydrate to accelerate the wound healing process and cost-effectively treat *S. aureus*-induced (resistant) skin infections.[47] Similarly, Kamal et al have used the cephalexin antibiotic, which has been loaded into poly(3-hydroxy butyric acid-co-3-hydroxy valeric acid) nanofibers, demonstrating an antibacterial activity both in vitro and in vivo in diabetic mice model against methicillin-resistant *S. aureus* (MRSA).[48]

Fus is another antibiotic that has been integrated with polylactic glycolic acid (PLGA) nanofiber and showed activity against wound-colonized bacteria including *Pseudomonas aeruginosa* (*P. aeruginosa*), and MRSA.[44] In addition, TGF-β1-inhibitor has been incorporated into poly(ε-caprolactone) (PCL)/gelatin (PG) co-electrospun nanofibrous scaffold, which has been shown to inhibit fibroblast generation and prevent scar formation in healing wounds.[45] Moxi antibiotic was also incorporated in CS and polyethylene oxide (PEO) nanofibers, which showed antimicrobial activity against *S. aureus, Escherichia coli* (*E. coli*), and *P. aeruginosa*, and wound healing efficacy.[49] Previous studies have explored the utilization of Pir in nanofiber applications for wound healing purposes. For example, a recent investigation conducted by Tottoli et al[50] incorporated Pir into nanofiber systems consisting of PLA-PCL, which were used as dressings. Their findings demonstrated the drug's antifibrotic effects on hypertrophic scar fibroblasts (HSFs), thus highlighting the potential of biofiber as an effective therapeutic approach for hypertrophic scar treatment within the context of wound healing. Furthermore, Tawfik et al demonstrated the antibacterial activity of a Moxi/Pir-loaded PLGA/PVP coaxial nanofiber system in the treatment of rabbit corneal infections.[36]

Considering that infection and inflammation can interfere with and delay normal wound healing, a combination of antibiotic and anti-inflammatory drugs can be an effective way of expediting wound healing. Thus, here we aim to develop coaxial electrospun nanofiber mats loaded with antibiotics, either Moxi, Fus, or Pir (as an anti-inflammatory) with the ability to be released directly on an injured site to prevent bacterial growth, minimize the inflammation, and thus accelerate wound closure.

Materials and Methods

Materials

PVP with an average molecular weight of 1,300,000, Moxi hydrochloride, Fus sodium salt, formic acid (98–100% for LC-MS LiCropur) and ethanol (absolute, ≥99.8%) were all obtained from Sigma-Aldrich (St. Louis, MO, USA), while Pir was brought from TCI chemicals (Toshima, Tokyo, Japan). Acetonitrile (CHROMASOLV, ≥99.9% for LC-MS) was purchased from Fisher Scientific (Waltham, MA, USA), and distilled water was generated from Milli Q, Millipore (Billerica, MA, USA).

Fabrication of Core/Shell Fibers

The coaxial fibres were prepared using Spraybase® (Dublin, Ireland) based on a modified method of Alkahtani et al and Alshaya et al.[51,52] The core polymer solution was prepared by dissolving 8% (w/v) of PVP in absolute ethanol and kept stirring at room temperature for 1 hour and then 0.5% (w/v) of Pir was added and stirred until complete dissolving. For the shell solution, 8% (w/v) PVP was also dissolved in ethanol with either 0.5% (w/v) Moxi or Fus and magnetically stirred at room temperature until completely dissolved. The prepared electrospun solutions were loaded into two 5 mL syringes and connected to a coaxial needle with an inner diameter of 0.45 mm and an outer diameter of 0.9 mm. The coaxial fibers of Moxi/Pir were produced at a constant voltage of 9.50 kV using a flow rate of 0.8 mL/hour for both core and shell solutions and a tip-to-collector distance of 15 cm. The coaxial fibers of Fus/Pir were produced using the same parameters but at a constant voltage of 9.00 kV. The electrospinning processes were carried out at room temperature with a relative humidity of 40%. Blank fibers were prepared with 8% (w/v) PVP solution both in the core and in the shell without the addition of any drug using the same electrospinning parameters but at a constant voltage of 7.00 kV.

Analysis of Fibers Morphology by Scanning Electron Microscopy (SEM) and Transmission Electron Microscopy (TEM)

The surface morphology of the electrospun nanofibers was analyzed using JEOL SEM (JSM-IT500HR, ASIA PTE. Ltd., Singapore). In preparation for imaging, samples were placed on SEM stubs using carbon tape and next coated with platinum (2 nm thickness) using the Auto Fine Coater (JEC-3000FC, JEOL, ASIA PTE. Ltd., Singapore). The average fiber diameters were measured from 50 different fibers using ImageJ software (National Institute of Health, MD, USA). The core and shell layers were distinguished via TEM (JEM-1400 TEM, JEOL, Tokyo, Japan) at an accelerating voltage of 80 kV by collecting the fibers directly onto a copper grid while electrospinning.

Fourier-Transform Infrared Spectroscopy (FTIR) Analysis

Thermo smart ATR IS20 Spectrometer (Thermo Fisher Scientific, Waltham, MA, USA) FTIR analyzer was used to determine the components and molecular structures of drug-loaded and blank fibers, as well as the pure PVP, Moxifloxacin, Pirfenidone, Fusidic Acid, and their physical mixture (PM). Both PM Moxi/Pir and PM Fus/Pir were prepared individually in a ratio of 16:1 from PVP: Moxi/Pir and PVP: Fus/Pir, respectively. The spectral resolution of 4 cm^{-1} was used to obtain the FTIR spectra of the samples at a wavenumber between 4000 and 600 cm^{-1}, and 32 scans were taken for each sample.

X-Ray Diffraction (XRD) Analysis

Rigaku Miniflex 300/600 (Tokyo, Japan) with Cu Kα radiation (λ = 1.5148 227 Å) and a voltage of 40 kV and a current of 15 mA was used to evaluate the crystallinity of PVP, Moxi, Fus, Pir, PM Moxi/Pir, PM Fus/Pir, blank and drug-loaded nanofibers. After placing the samples on aluminum trays, the XRD patterns were scanned at a speed of 5°/minute across the diffraction angle (2θ) range between 2° and 60°.

Disintegration Test of Nanofiber Systems

A modified method described by Almuwallad et al[53] was used to evaluate the disintegration of Moxi/pir nanofibers, Fus/pir nanofibers, and blank fibers. 2×2 cm of fibrous mats were placed in a petri dish containing 8 mL of distilled water at room temperature until detachment was completed. The results represent the average ± standard deviation (SD) of three replicates.

Drug Quantification by High-Performance Liquid Chromatography (HPLC)

The HPLC quantification of Moxi, Pir, and Fus was performed on a 1260 Infinity II HPLC system (Agilent, Santa Clara, CA, USA) comprising an autosampler with column oven compartment (G7129A), a binary solvent gradient flexible pump (G7111A), and a UV detector (G7114A). The HPLC separation of the drugs was accomplished using an Agilent HPLC column Poroshell 120 EC-C18 (4.6 mm × 150 mm, 4 μm) column, with a temperature set as ambient temperature. The mobile phase was an LC/MS grade water plus 0.1% formic acid (A) and acetonitrile plus 0.1% formic acid (B). At a flow rate of 0.40 mL/min, a linear gradient program with a total runtime of 15 minutes was used as follows: 0.0–2.0 min 5% (B), 2.0–10.0 min from 5% to 95% (B), 10.0–11.0 min 95% (B), 11.0–12.0 min from 95% to 5% (B) and finally 12.0–15.0 min 5% (B) and injection volume 10 μL. Moxi, Pir, and Fus were identified and detected at retention times Rt = 8.9 min (295 nm), 10.0 min (315 nm), and 14.2 min (223 nm), respectively, as shown in Supplementary Figure 1. Calibration curves were constructed using a series of concentrations ranging between (100–0.4 μg/mL) which is shown in Supplementary Figure 2A for Moxi and Pir and 2B for Fus and Pir. Data analysis was processed using OpenLab CDS software.

Quantification of Encapsulation Efficiency (EE%) and Drug Loading (DL)

Certain amounts of the dual drug-loaded fibrous system were dissolved in 10 mL PBS pH 7 and kept at room temperature until complete dissolving. The actual amount of Moxi, Pir and Fus were determined using the above-developed HPLC method, and the EE% and DL were determined by the following equations:

$$Encapsulation\ Efficiency\,\% = \frac{Actual\ drug\ amount}{Theoretical\ drug\ amount} \times 100 \quad (1)$$

$$Drug\ loading = \frac{Entrapped\ drug\ amount}{Fibers\ Weight} \quad (2)$$

The results represent the average ± SD of three replicates.

In vitro Drug Release by Franz Diffusion

In vitro, release of the drugs from the prepared nanofibers was studied using the Franz diffusion cell system (PermeGear, Hellertown, PA, USA). A piece of a semipermeable membrane (Spectra/Por®, Spectrum Laboratories Inc., Ranch Dominguz, CA, USA) with a molecular weight cut-off of 12–14 kD, was placed over each Franz cell. Phosphate-buffered saline PBS (pH 7) was used to fill the receptor compartments. One mL of PBS was added to each donor compartment. The system was maintained at 37 ± 0.02°C via a circulating water bath to mimic skin surface temperature, and the diffusion medium was stirred at 600 RPM. Certain amounts of the nanofiber samples were placed on the donor side, and the open ends of the Franz cells were covered with parafilm® to prevent evaporation. At predetermined time points up to 24 hours (0.5, 1, 2, 4, 6 and 24 hours), a 100 µL sample was withdrawn from the receptor compartment (containing 3 mL PBS pH 7) and replaced by fresh buffer to maintain the sink conditions. The withdrawn samples were analyzed by the developed HPLC method, and the cumulative amount of drug release was calculated according to the following equation:

$$Cumulative\ release\,\% = \frac{Cumulative\ drug\ amount}{Theoretical\ drug\ amount} \times 100 \quad (3)$$

The results represent the average ± SD of three replicates.

Determination of the Minimum Inhibitory Concentration (MIC) of the Pure Drugs

A total of four ATCC bacterial strains were used including *S. aureus* ATCC 29213 and ATCC BAA-977, *P. aeruginosa* ATCC 9721, and ATCC 27853 cultured in Muller-Hinton agar media and incubated at 37°C overnight. The MIC for Moxi, Fus and Pir were determined in Muller-Hinton broth using microdilution plates. Serial dilutions of drugs were prepared for Fus and Pir (1024, 512, 256, 128, 64, 32, 16, 8, 4, 2, 1, 0.5 µg/mL) and (256, 128, 64, 32, 16, 8, 4, 2, 1, 0.5, 0.25, 0.125, 0.0625 µg/mL) for Moxi in Muller-Hinton broth and added to 96-well plates. Then, the bacterial suspensions were added to each well to achieve a final inoculum of 1×10^6 CFU/mL. All 96-well plates were incubated at 37°C overnight with a continuous shaking speed at 140 RPM. The endpoint of MIC was measured at absorbance (600 nm) using CytationTM 3 Cell Imaging Multi-Mode Reader (BioTek Instruments, Winooski, USA).

Determination of the Antibacterial Activity of the Dual Drug-Loaded Coaxial Fibers

The antibacterial effectiveness of the prepared coaxial nanofibrous systems was evaluated by the zone of inhibition assay. A certain weight of the dual drug-loaded fibers was placed in the Petri dishes that contained a final inoculum of 1×10^6 CFU/mL from each bacterium (*S. aureus* and *P. aeruginosa*). Drug-loaded discs were used as positive control, which contained a similar drug amount to the drug-loaded fibers, while blank (drug-free) fibers at a similar fibrous mat weight to the drug-loaded fibers were used as a negative control. The fibers and discs were loaded in the center of each Petri dish, and the dishes were incubated at 37°C overnight.

Determination of the Inhibitory Concentration (IC) of the Pure Drugs

Human dermal fibroblasts (HFF-1; ATCC SCRC-1041, Homo sapiens) were used to assess the IC_{20} and IC_{50} according to a modified method of Tawfik et al[36] and Alshaya et al[52] The cells were sub-cultured and maintained in Dulbecco's modified eagle medium (DMEM), supplemented with 10% (v/v) fetal bovine serum (FBS), Penicillin 100 U/mL, and Streptomycin 100 µg/mL, all obtained from Sigma-Aldrich (St. Louis, MO, USA). MTS reagent (cell titer 96® aqueous one solution cell proliferation assay, Promega, Southampton, UK) was used to conduct the MTS cytotoxicity

assay on a living cellular model (passage = 12). HFF-1 cells were harvested with 0.25% Trypsin-EDTA, counted with trypan blue exclusion test, and seeded to a 96-well plate at a seeding density of 1×10^4 cells/well. The seeded cells were incubated overnight in a humified 5% CO_2 cell culture incubator at a temperature of 37°C. After reaching around 50% to 60% confluency, 100 µL of DMEM that contained the tested drugs: Moxi, Fus alone or in combination with Pir and Pir only at a serial dilution range from 500 to 15.6 µg/mL, were then incubated with the cells for 24 hours. Untreated cells and 0.1% triton x-100 treated cells were the positive and negative controls used in this assay, respectively. Following the 24-hour incubation period, the mixture was aspirated from each well and a combination of DMEM and MTS reagent (4:1) with a total volume of 100 µL was added and incubated for 3 hours in a dark biosafety cabinet at 37°C. The color intensity of each well was measured at 490 nm via Cytation 3 absorbance microplate reader (BIOTEK Instruments Inc., Winooski, VT, USA). Finally, the cell viability percentage was calculated using the following equation:

$$Cell\ viability\,\% = \frac{(S-T)}{(H-T)} X100 \tag{4}$$

whereas S, T, and H represent the absorbance of the cells treated with the tested drug, the absorbance of the cells treated with triton x-100, and the absorbance of the cells treated with DMEM. The results represent the average (± SD) of three replicates.

In vivo Diabetic Model

Thirty-two male Wistar rats weighing 250 ± 30 gm were obtained from the animal house, College of Pharmacy, King Saud University. Animals were maintained in a temperature-controlled room at 25°C and an average relative humidity of 50% in a 12:12 h light/dark cycle. All animal experiments strictly followed the guidelines of the Ethical Committee for Performing Studies on Animals, King Saud University, Riyadh, Saudi Arabia, protocol number KSU-SE-22-5. Rats were randomly divided into 8 groups (n = 4) and after an overnight fasting received a single 65 mg/kg intraperitoneal injection of streptozotocin (STZ; Sigma-Aldrich, Taufkirchen, Germany). After 72 hours, rats with a fasting blood glucose level of 250 mg/dL or higher were considered diabetic. Supplementary Figure 10 shows the rats' blood sugar before and throughout the study.

Treatment Application and Measurement of Wound Size

On the day of wound excision, rats were anesthetized using 3% isoflurane, back hair was removed using an electric clipper, and the wound was excised using a sterilized scalpel. Rats were then randomly divided into 8 groups (n = 4) and either received blank fibers, Moxi/Pir fibers, Fus/Pir fibers, Pir fibers, Moxi fibers, or Fus fibers. Fibers were secured in place using 3M™ Tegaderm™ transparent film. One group of rats received the commercially available 10% Povidone Iodine (ie, PVP-I) non-adherent dressing, under the brand name of INADINE®, as a treatment-positive control, and one group of rats received no treatment and served as a disease control. Animals were treated once daily for 14 days or until total wound closure. Wound swab was taken before treatments and on days 0, 1, 3, 5, 7, 9, 11 and 13 post-treatments. Changes in wound appearance were monitored through taking photos of before and throughout the study and the wound sizes were measured using a micrometer-electronic digital caliper. Animal weight was also monitored, as shown in the Supplementary Figure 9. Statistical analysis was performed using one-way ANOVA and Tukey's post-hoc test. GraphPad Prism software (GraphPad Software Inc., San Diego, CA, USA) was used for statistical analysis and graph plotting.

In vivo Microbial Total Count

Following the wounding of the rats participating in the experiment, and before the addition of treatments, standard bacterial swabs were taken from their wounds on the start day and then were collected from each group on days 0, 1, 3, 5, 7, 9, 11, and 13. The swabs were then placed into a sterile tube containing 1 mL of phosphate-buffered saline (PBS) to prepare a 1:10 dilution and spread on a Petri dish. The plates were incubated for 24 to 48 hours at 37 °C. Then, the transplanted colonies were counted and reported.

Histopathological Assessment of the Wounds

At the end of the study, animals were sacrificed using a CO_2-filled chamber with a flow rate of 30–70% per minute for 5 minutes, and then wound or skin was trimmed and fixed in 10% formalin for 48 hours. To dehydrate the tissues, 70% ethanol was used, and tissues were then sent to the Department of Pathology, College of Medicine, King Saud University for Hematoxylin and Eosin staining (H&E). The histology of skin tissues for both treated and non-treated animals was examined by a pathologist, using light microscopy.

Statistical Analysis

The EE%, DL, drug release studies, and in vitro experiments were all conducted with three independent replicates, and the data are presented as the average ± SD. Statistical analysis was performed using OriginPro® 2021 (OriginLab Corporation, Northampton, MA, USA) and Microsoft Excel 2024 software. For the statistical analysis of in vivo experiments, one-way ANOVA and Tukey's post-hoc test was employed, and GraphPad Prism software (GraphPad Software Inc., San Diego, CA, USA) was used for both statistical analysis and graph plotting, where the p-values of <0.05 were considered statistically significant.

Results and Discussions

Analysis of Fibers Morphology by Scanning Electron Microscopy (SEM)

The surface morphologies of both the prepared coaxial fibers and blank nanofibers had a uniform and smooth surface without beads as shown in Figure 1. The blank nanofiber has a diameter of 760 ± 105 nm, while Moxi/pir fiber mats and Fus /pir mats were measured to be 443 ± 67 nm and 488 ± 92 nm, respectively. The larger diameter for the blank fibers was attributed to the lower voltage (ie, 7 kV) that was used compared to the dual drug-loaded fibers (ie, ≥9 kV) which stabilized the spinning jet and allowed for larger diameter fibers.[54] A similar observation was demonstrated in the imeglimin-loaded PVP nanofibers of Alamer et al[55]

The core and shell layers were distinguished using the TEM as shown in Figure 2. This was in agreement with Alkahtani et al and Alshaya et al who demonstrated a similar observation for their PVP/PVP coaxial nanofibrous systems.[51,52] Due to the miscibility of the core and shell polymer solutions, which were both at the same concentration (8% w/v) and the flow rate was kept constant at 0.8 mL/hour, the thickness of the inner layer appeared considerably large (as shown in Figure 2). The reason that the fibers were prepared using the coaxial needle was to avoid loading a high concentration of drugs (1% w/v, ie, equally divided for each drug) into single-layered (monoaxial) fibers, which would reduce the drug-to-polymer ratio, preventing the encapsulation of the drugs and accelerate their release. In addition, owing to the ultrarapid disintegration of the PVP fibers, this delivery system will be used as a drug delivery system and not as a medicated fibrous scaffold. Overall, the successful preparation of this coaxial system was satisfying to further test the fibers using in vitro and in vivo tests.

Fourier-Transform Infrared Spectroscopy (FTIR) Analysis

The FTIR is considered one of the easiest and fastest techniques used to detect the important functional groups for each sample and gives an initial indication of any specific molecular interactions between the samples. Thus, the compatibility of the drugs and the polymer was tracked using FTIR spectroscopy to assess any structural changes that might have occurred due to the drugs' incorporation with PVP and to assure the stability of the resulting formulation. Table 1 summarizes the most characteristic FTIR peaks of all pure materials (PVP, Moxi, Fus, Pir) based on the FTIR spectrum in Figure 3. The presence of C-N vibrations from pyrrolidone around the 1280 cm^{-1} region and the strong C=O band at 1638 cm^{-1} in the FTIR spectra of PVP, blank fiber, drug-loaded fibers, and the PMs led to the inference that PVP polymer was present. In addition, the presence of a broad O-H stretching peak at 3430 cm^{-1}, owing to the hygroscopic nature of PVP, provides additional evidence for the presence of the polymer. The PVP findings align with what was found by Alshaya et al[52]

The PM Moxi/Pir spectrum in Figure 3 displayed low-intensity peaks related to the PVP and the drugs. The PVP polymer was indicated by peaks at 1652, 1423, and 1279 cm^{-1}, while Moxi and Pir peaks appeared at a lower intensity

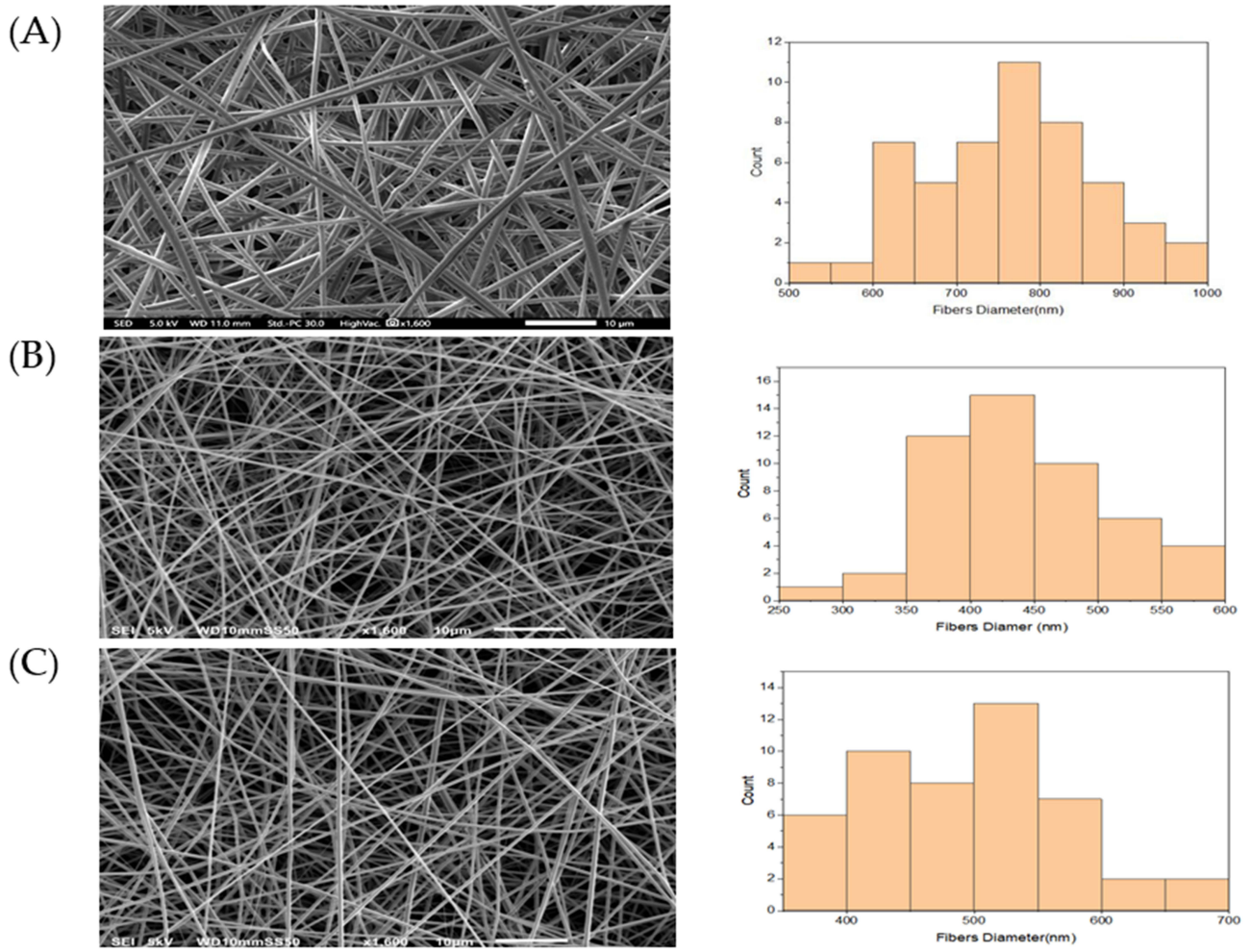

Figure 1 Surface morphologies of the drug-loaded coaxial fibers (**A**) blank, (**B**) Moxi/Pir, and (**C**) Fus/Pir nanofibers and their corresponding diameter distribution.
Notes: The SEM images showed uniform and un-beaded fibers with a diameter of 760 ± 105 nm, 443 ± 67 nm and 488 ± 92 nm, respectively. The size distribution of the drug-loaded core/shell nanofibers was measured from 50 different fibers.
Abbreviations: Moxi, moxifloxacin; Fus, fusidic acid; Pir, pirfenidone.

within the fingerprint region, corresponding to the polymer-to-drug ratio (16:1). Moreover, the drug-loaded fibers in Figure 3 exhibited peaks related to Moxi and Pir, including a C=C peak at around 1500 cm^{-1}, stretching vibration of phenyl fluoride at 1181 cm^{-1}, and intense peaks that were detected in the fingerprint region at approximately 1003, 932, 891, and 649 cm^{-1} corresponding the C–H from substituted benzene. These results are consistent with the previously published findings of Tawfik et al.[59]

The FTIR of the second PM of Fus/Pir in Figure 3 showed high-intensity peaks that represent the PVP at 1651, 1495, 1456,1422, 1370, 1283, and 1271 cm^{-1}, while less-intense peaks represented the drugs at 1557 and 1338 cm^{-1} as a result of C=C stretching of and C-H bending, respectively. On the other hand, the intensity increase of the peaks, especially at 3650–3100 cm^{-1} and 1650 cm^{-1} in the drug-loaded fibers in Figure 3 due to the stretching vibrations of O-H and C=O for PVP and Fus, in addition to the peaks presented in the PVP polymer and the blank fibers at 1492, 1459, 1436, and 1421 cm^{-1} for the C-H bending vibration and 1286 cm^{-1} for the pyrrolidone stretching vibration. Fus and Pir in the DL fibers also exhibited many low-intensity peaks at 1018, 1001, and 930 cm^{-1} in the fingerprint region, which could correspond to the C-H from substituted benzene and C=C-H vibrations.

As described in numerous studies, these observations for both drug-loaded fibers demonstrate the compatibility of the drugs with PVP without any chemical interactions. Aburayan et al demonstrated the absence of any changes in the chemical structure or interaction between the Halicin and PVP nanofibers after the electrospinning process.[62]

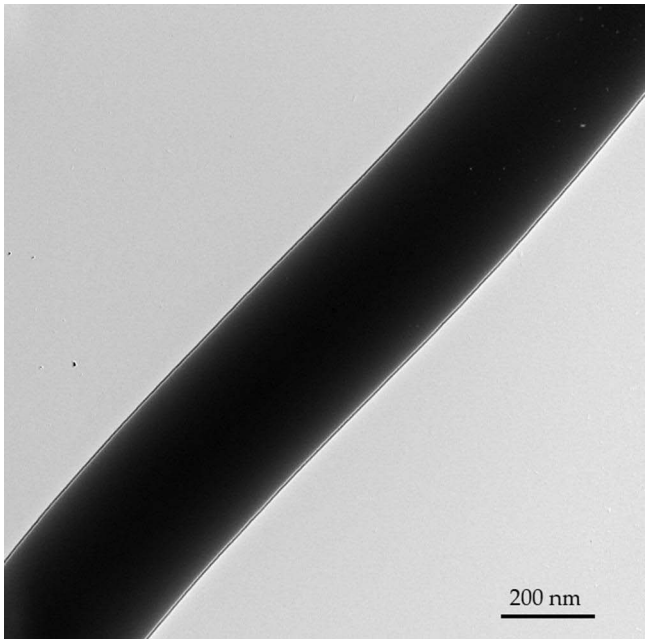

Figure 2 A representative TEM image showing the two distinctive layers of the inner and outer layers of this PVP/PVP nanofibrous system.

Furthermore, the PVP nanofibers preserved the characteristic properties after loading albendazole sulfoxide and praziquantel drugs by Gültekin et al, which indicates the compatibility between drugs and PVP through electrospinning.[63]

X-Ray Diffraction (XRD) Analysis

XRD was used to determine the drug's crystallinity and to assess the amorphous state of the solid dispersion as illustrated in Figure 4. The XRD pattern of PVP demonstrated a broad-halo peak due to the amorphous nature of the PVP polymer, with no crystalline peaks expected to be observed, as well as in the blank fibers. This is consistent with the findings

Table 1 FTIR Characteristic Peaks of the Pure PVP (Polyvinyl Pyrrolidone), Moxi (Moxifloxacin); Pir (Pirfenidone); and Fus (Fusidic Acid)

Sample	Peak Wavenumber (cm^{-1})	Characteristic Peak Description	Ref.
PVP	3650–3100	Stretching vibration of O-H from the hygroscopic nature of PVP	[52,56]
	1644	Stretching vibration of C=O	
	1421, 1457, 1490	Bending vibration of aliphatic C-H	
	1283	Stretching vibration of C-N from pyrrolidone.	
Moxi	3525	Stretching vibration of O-H	[57–59]
	3465	Stretching vibration of secondary amine N-H	
	1181	Stretching vibration of C-F from monoflourobenzene	
	1621, 1515, and 1452	Stretching vibration of aromatic C=C	
	1350	Asymmetric stretching of C-N from aromatic amine	
	1702	Stretching vibration of C=O from the carboxylic acid	
	873, 803, 719	Bending vibration of C-H from substituted benzene	

(*Continued*)

Table 1 (Continued).

Sample	Peak Wavenumber (cm^{-1})	Characteristic Peak Description	Ref.
Pir	3051	Stretching vibration of aromatic C-H	[59,60]
	2927	Stretching vibration of alkene C-H	
	1671	Stretching vibration of C=O from tertiary amide	
	1608–1454	Stretching vibration of aromatic C=C	
	1272	Stretching vibration of C-N from tertiary amine	
	868, 822, 763, 699	Bending vibration of C-H from substituted benzene	
Fus	3477	Stretching vibration of O-H	[61]
	2934 and 2865	Symmetrical and asymmetrical stretching of C-H	
	1550	Stretching vibration of C=C	
	1376	Bending vibration of C-H from the methyl group	
	1709 and 1650	Symmetrical and asymmetrical stretching of C=O	
	1269	Stretching vibration of C-O	
	974	Vibration of C=C-H	
	920 and 855	Vibration of C-H	

published by Alkahtani et al.[51] The XRD of the pure Pir, Moxi, and Fus drugs exhibited crystallinity forms, as evidenced by the presence of several narrow and intense Bragg reflection peaks in their XRD patterns. The Pir pattern (Figure 4) showed distinctive Bragg reflections that confirm its crystalline nature at 2θ values of 8.85°, 14.43°, 15.4°, 18.63°,

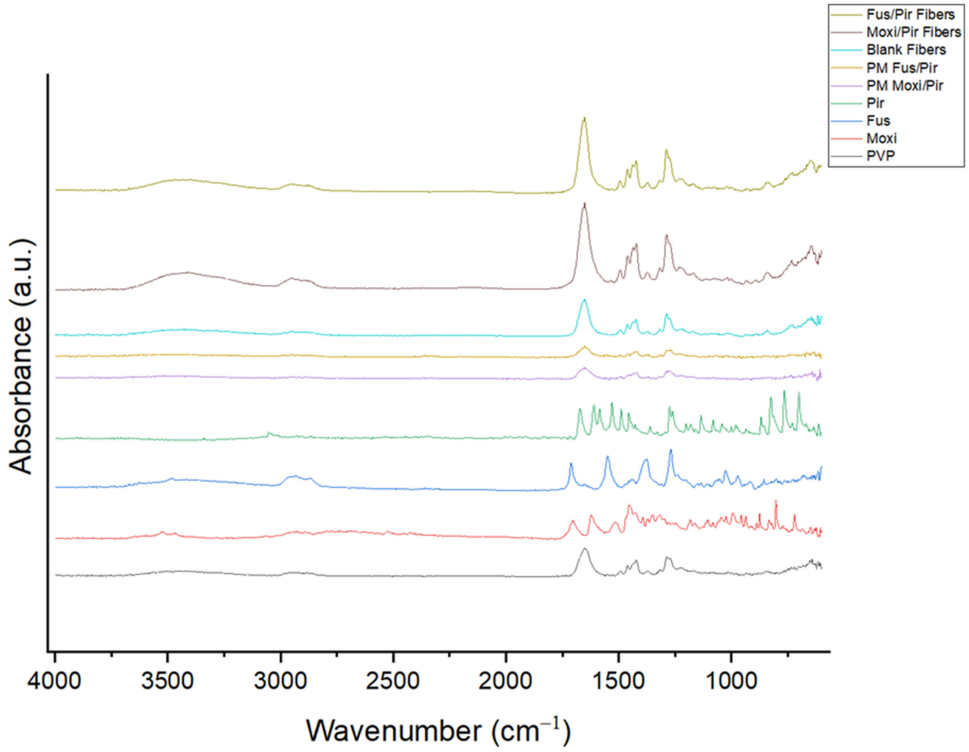

Figure 3 FTIR spectrum of PVP, Moxi, Fus, Pir, PM Moxi/Pir, PM Fus/Pir, blank and drug-loaded nanofibers.
Abbreviations: Moxi, moxifloxacin; Fus, fusidic acid; Pir, pirfenidone; PM, physical mixture; DL, drug-loaded.

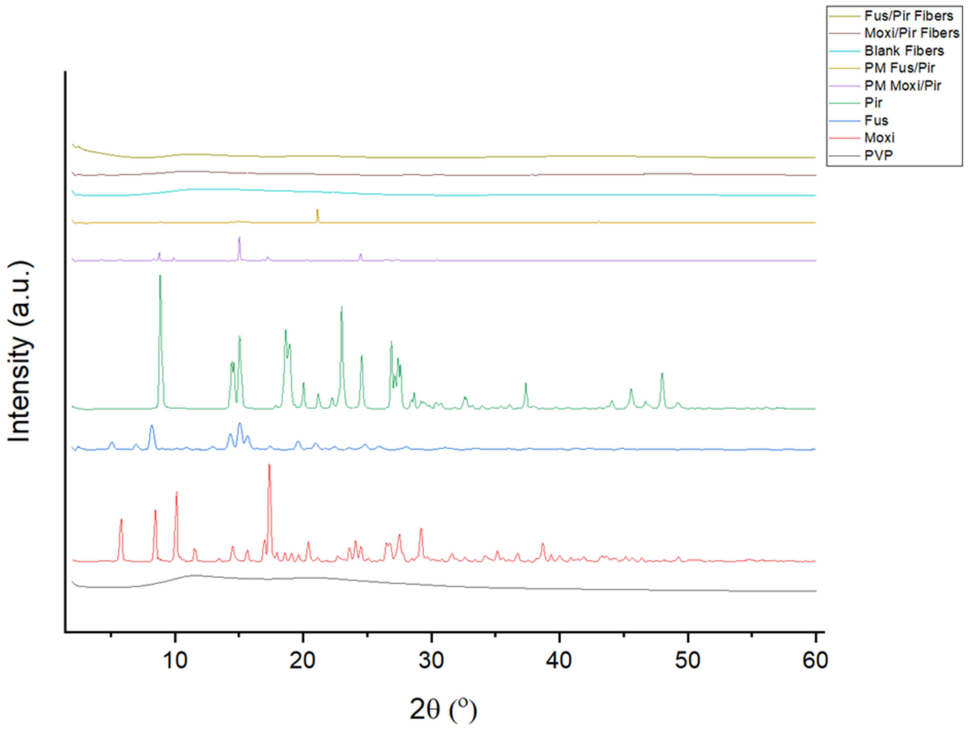

Figure 4 XRD patterns of PVP, Moxi, Fus, Pir, PM Moxi/Pir, PM Fus/Pir, blank and drug-loaded nanofibers.
Abbreviations: Moxi, moxifloxacin; Fus, fusidic acid; Pir, pirfenidone; PM, physical mixture; DL, drug-loaded.

18.97°, 22.99°, 24.59°, 26.86°, 27.44°, 37.38°, 45.57°, and 48.03°. These findings align with published results of Borhade et al.[64] Additionally, Moxi pattern also exhibited intense peaks at 5.84°, 8.48°, 10.13°, 17.37°, and 29.22° indicating its crystallinity nature, which is consistent with Tawfik et al[59] and Shah et al.[65] As shown in PM Moxi/Pir pattern (Figure 4), Moxi and Pir peaks were observed at diffraction angles of 5.66°, 8.80°, 9.93°, 15.04°, 17.21°, and 24.49°.

Furthermore, Figure 4 presents the diffractogram of the second formulation, which signified the crystalline structure of Fus at 5.05°, 6.93°, 8.17°, 14.30°, 15.02°, 15.67°, 19.55°, 21°, and 24.81°, similarly to Thakur et al,[66] and Gilchrist et al.[67] Both Fus and Pir peaks were observed at the PM Fus/Pir at 8.08°, 8.81°, 14.95°, 21.13°, and 43.06° but in a very low intensity. The presence of the low-intensity peaks in both PMs, while they were lacking in the drug-loaded fibers (displayed broad-halo), confirms the molecular transformation of the drugs after being. These findings agreed with the results in numerous studies that confirm the transformation of the drug's crystallinity to an amorphous state due to the electrospinning process.[62,68,69]

Disintegration Test of Nanofiber Systems

The disintegration was measured to be ≤2 seconds for all tested nanofiber systems, ie, blank, Moxi/Pir, and Fus/Pir nanofibers, as demonstrated in Figure 5. Both Alkahtani et al and Bai et al exhibited a similar ultrafast disintegration of the drug-loaded PVP nanofibers, which is attributed to the hydrophilic and hygroscopic nature of the PVP polymer.[51,70]

Quantification of Encapsulation Efficiency (EE%) and Drug Loading (DL)

The amount of encapsulated drugs and the drug loading of the prepared coaxial nanofibers were determined using a developed HPLC-UV system, using predetermined calibration curves, as shown in Supplementary Figure 2A for Moxi and Pir and 2B for Fus and Pir. The EE% and DL for the Moxi/Pir nanofibers were measured to be 70 ± 3% and 20 ± 1 µg/mg, respectively, for Moxi, and 96 ± 6% and 28 ± 2 µg/mg, respectively, for Pir.

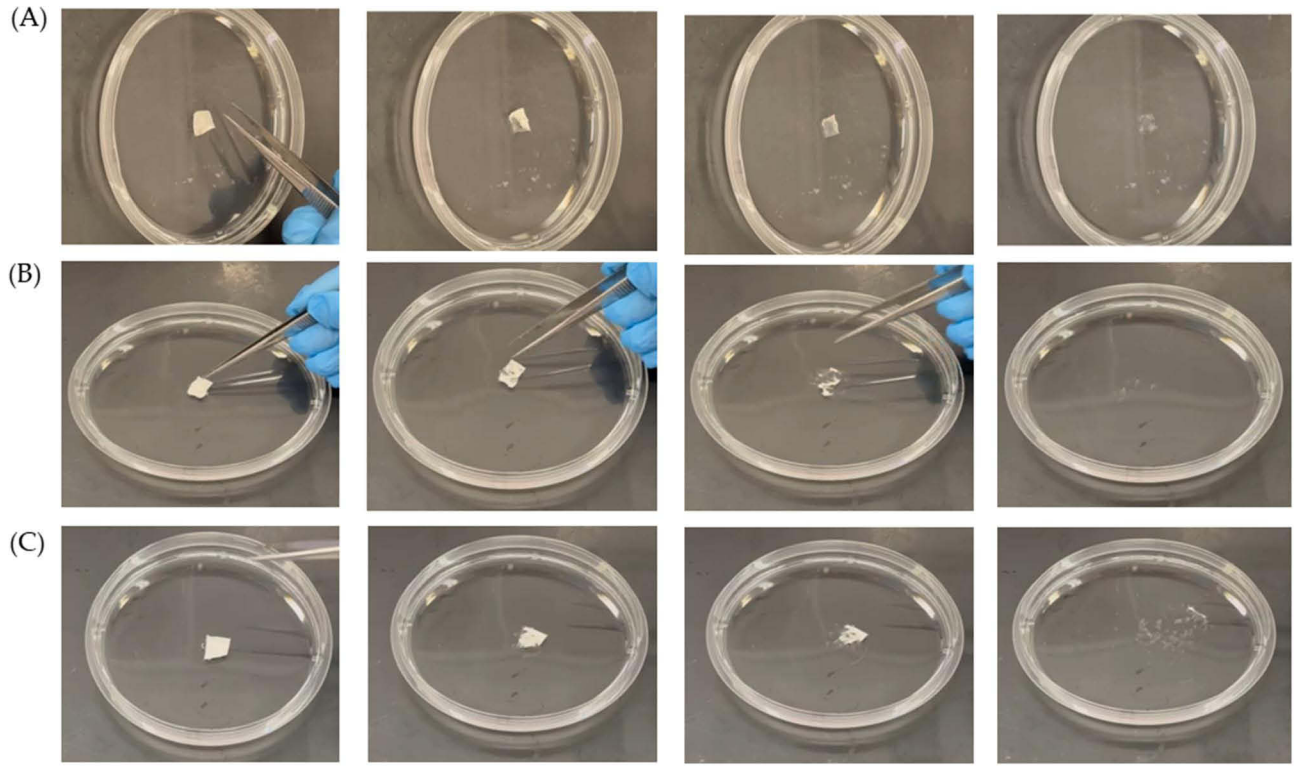

Figure 5 Disintegration test of (**A**) blank nanofibers, (**B**) Moxi/Pir nanofibers, and (**C**) Fus/Pir nanofibers.
Notes: All nanofiber systems disintegrated ≤2 seconds (n = 3).

The EE% of Pir was very close to the theoretical amount (100%), whereas the EE% of Moxi was lower, which needs further investigation. Different studies have shown a highly encapsulated Moxi in hydrophilic polymer systems including Hameed et al who showed about 100% encapsulation of the Moxi loaded into CS: PEO nanofiber system.[49] Tawfik et al have also shown a high EE% of 87.5 ± 3% and 80 ± 2%, respectively, for the Moxi/Pir-loaded PVP/PLGA nanofiber system.[59] The corresponding EE% and DL for the Fus/Pir-loaded into coaxial PVP fibers were 95 ± 6% and 28 ± 2 μg/mg, respectively, for Fus, and 102 ± 5% and 30 ± 2 μg/mg, respectively, for Pir. Both drugs were highly incorporated into the nanofiber probably due to the high solubility and miscibility of the drug solutions in the preparatory step.

In vitro Release Franz Diffusion Studies

The in vitro drug release profiles of the dual drug-loaded nanofiber systems were performed using a Franz diffusion cell system using PBS (pH 7). In the first coaxial system, PVP: Moxi (shell)/PVP:Pir (core), both drugs had a similar release pattern as shown in Figure 6A. The released amount of Moxi and Pir at the first 30 minutes were 19% and 26%, respectively, reaching to 34% and 40%, respectively, after the first 2 hours. Pir, however, reached a higher release amount of 71% in 6 hours compared to 57% for Moxi. Both drugs were released completely after 24 hours. PVP is a hydrophilic polymer, which is highly soluble in hydrophilic solutions. Also, Moxi and Pir are highly soluble drugs. Therefore, the drug release profile of both drugs was similar owing to the miscibility of nanofiber system components, in addition to the use of the same concentration of polymers and drugs in the preparation of this nanofiber system. Different studies have incorporated multiple drugs in the coaxial nanofiber system including Tawfik et al[59] who incorporated Moxi as a core and Pir as a shell on PVP/PLGA nanofiber system. They had a high-release profile, which reached 100% of Pir and 70% Moxi in 24 hours. This study showed a lower release of Moxi than this current study, possibly due to the location of the drug in the core and the outer layer of PLGA could decrease the amount of drug released. In another study, the use of a hydrophilic nanofiber system such as the combination of CS and PEO effectively delivered Moxi, demonstrating

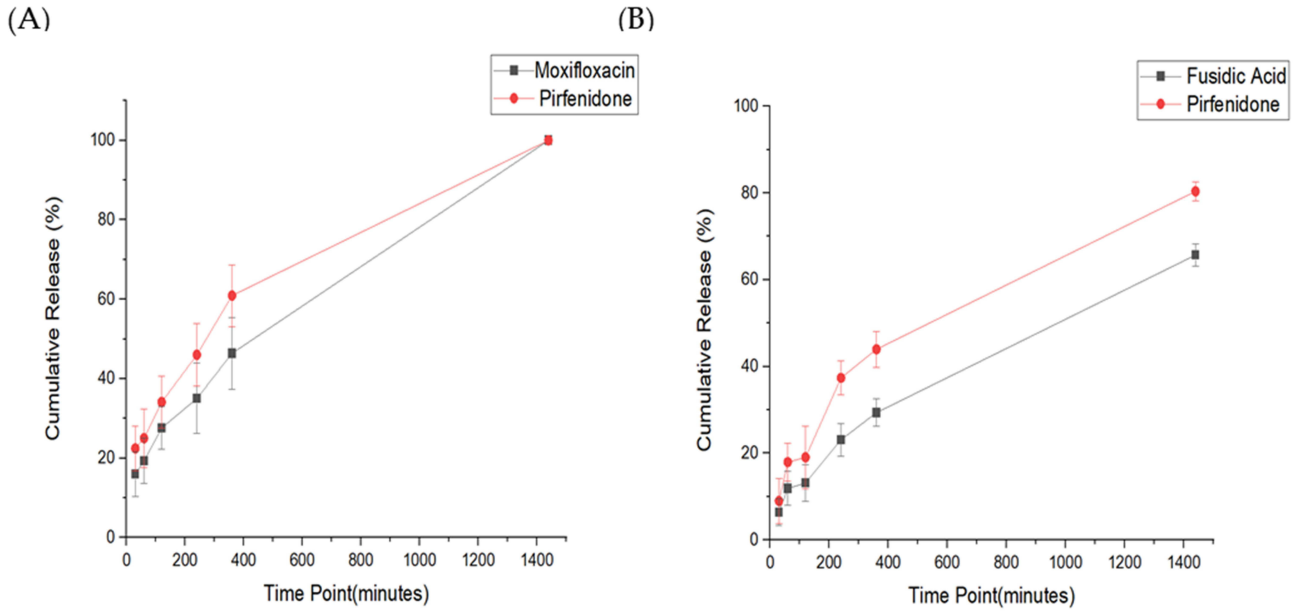

Figure 6 In vitro release profile of (**A**) Moxi/Pir-loaded coaxial nanofibers and (**B**) Fus/Pir-loaded coaxial nanofibers.
Notes: Results represent the average ± SD (n = 3).
Abbreviations: Moxi, moxifloxacin; Fus, fusidic acid; Pir, pirfenidone.

a release rate of 79.8 ± 4.2% within 48 hours at pH 7.4. Although their sustained-release profile persisted for a longer duration, the amount of encapsulated drugs in their system exceeded this current study, falling within the range of 99–101%. Comparatively, our nanofiber system achieved 100% drug release within 24 hours at pH 7, but with an encapsulation efficiency of 67%, while, the study achieved approximately 60% drug release within the first 24 hours but with an EE% of 99–101%.[49]

On the other hand, the release of the other coaxial nanofibrous system, ie, PVP:Fus (shell)/PVP:Pir (core) demonstrated a similar release profile for both drugs, as shown in Figure 6B. After 4 hours, 23% of Fus and 37% of Pir were released, followed by 29 and 44%, respectively, after 6 hours, and finally, 65% and 80%, respectively, after 24 hours. To the best of our knowledge, this study represents the first attempt to incorporate Fus into a hydrophilic nanofiber system. Considering the hydrophilic nature of both PVP and the drugs, it is anticipated that they will rapidly dissolve under in vitro sink conditions. However, a slower release of Fus was shown in previous studies by Almostafa et al[71] and Kinani et al,[49] for Fus-loaded hydrogel and nanoemulgel and Fus-loaded PVA/CS nanofibers, respectively, using the Franz diffusion system. It was reported in both studies that the solubility and Fus release rate might be affected owing to the degree of polymer matrix swelling, the polymer and/or excipient ratio, higher viscosity of the formulation and the polymer being behaved like a drug reservoir might slow down the release and diffusion of the loaded drugs.

Determination of the Minimum Inhibitory Concentration (MIC) of the Pure Drugs

Numerous factors can hinder the healing process in diabetic foot wounds, mainly bacterial colonization and wound infection.[72] Here, nanofibers loaded with antibiotics were used as wound dressings to treat the infection and help expedite the healing processes. The MIC assay was used to determine the antibacterial activity of the pure drugs, ie, Moxi, Fus and Pir against the most common pathogenic bacteria in diabetic foot wounds, the Gram-positive *S. aureus* and the Gram-negative *P. aeruginosa*.[73,74] The MIC values of Moxi against two different strains of *S. aureus*, ie, ATCC 29213 and ATCC BAA-977, were <0.5 µg/mL, whereas the MICs against two different strains of *P. aeruginosa*, ie, ATCC 9721 and ATCC 27853, were measured as 2 µg/mL and 4 µg/mL, respectively (Supplementary Figure 3 and Supplementary Table 1). Pir has shown no antibacterial activity against the pathogenic bacteria (Supplementary Figure 3 and Supplementary Table 1), which was in agreement with the result of Tawfik et al.[36] The MIC of Moxi was similar or within ± two-fold dilution to that of Tawfik et al,[36] which was 0.125 µg/mL against *S. aureus* and 4 µg/mL against *P. aeruginosa*, respectively. Speciale et al[75] also reported Moxi

activity against different strains of *S. aureus* in a range of 0.015–0.25 µg/mL or 1–2 µg/mL. In addition, Masadeh et al[76] reported an activity of Moxi against *S. aureus* ase 0.05 ± 0.02 µg/mL and against *P. aeruginosa* as 1.7 ± 0.7 µg/mL. However, the bacterial strains were different from those used in this current study.

The MIC of Fus was measured as <1 µg/mL against the two strains of *S. aureus* (ie, ATCC 29213 and ATCC BAA-977) and recorded a weaker activity of >512 µg/mL against the two strains of *P. aeruginosa* (Supplementary Figure 3 and Supplementary Table 1). These results were consistent with the results of Jones et al,[77] which reported a MIC ranging between 0.06 and 0.25 µg/mL against *S. aureus* ATCC 29213. Moreover, according to previous studies, Staphylococci are normally susceptible to Fus at MICs of ≤0.25, ≤0.5, or ≤1 µg/mL.[78–80] In addition, McGhee et al[81] have reported the MIC activity of 40 different *MRSA* strains isolated from cystic fibrosis patients to be 0.125 to 0.5 µg/mL, 0.5 µg/mL against *S. aureus* (HMC2230) and 0.25 µg/mL against *S. aureus* (HMC2232). Their MIC results against *P. aeruginosa* were also similar to this study, which were recorded to be >512 µg/mL against *P. aeruginosa* HMC461 and 256 µg/mL against *P. aeruginosa* HMC468. O'Brien et al[82] have also reported a more potent activity of Fus against *S. aureus* 25,923, which was 0.0156 µg/mL and a weaker activity of >256 µg/mL against *P. aeruginosa* PAO1.

Determination of the Antibacterial Activity of the Dual Drug-Loaded Coaxial Fibers

The antibacterial activity of the two dual drug-loaded coaxial nanofiber systems was evaluated using the zone of inhibition assay against the similar bacterial strains that were used in the MIC study, as shown in Table 2. Moxi is a broad-spectrum antibiotic that is effective against Gram-positive and Gram-negative bacteria.[33,34] Here, the antibacterial activity of Moxi/Pir nanofibers was tested using 1 mg of the fibers that contained 20 µg Moxi and 28 µg Pir compared to the blank fibers as a negative control and a similar amount of the drugs loaded into a microbiological disc, as a positive control. Similarly, 1 mg of the Fus/Pir nanofibers that contained 28 µg Fus and 30 µg Pir was tested.

The calculated zones of inhibition of Moxi/Pir-loaded nanofibers against *S. aureus* were 31 mm (ATCC 29213) and 38 mm (ATCC BAA-977), while they were 40 mm (ATCC 29213) and 41 mm (ATCC BAA-977) for the positive control (Table 2). On the other hand, a zone of inhibition of 25 mm and 30 mm were observed for this nanofiber system and positive control, respectively, against *P. aeruginosa* (ATCC 27853), and 10 mm for both the drug-loaded fibers and positive control against *P. aeruginosa* (ATCC 9721), as shown in Table 2. The blank fibers did not show any activity against the tested bacterial strains. This nanofiber system demonstrated a nearly identical zone of inhibition as the positive control (discs), which confirms the effectiveness of Moxi after being electrospun. The variation in the results between the fibers and the disc might be attributed to the deviation of the drug loading within the nanofibers. Various studies have incorporated Moxi antibiotics into different nanofiber systems to treat infections including Tawfik et al[36] who have incorporated this antibiotic into a PVP/PLGA coaxial nanofibrous system, and the study demonstrated a consistent result to this current study. Also, Hameed et al[49] have shown the effectiveness of CS and PEO nanofiber systems incorporated with Moxi in inhibiting the activity of *S. aureus, E. coli* and

Table 2 Zone of Inhibition of Moxi/Pir Nanofibers, Fus/Pir Nanofibers (Fus/Pir), and the Positive Controls (Drugs Loaded into Discs in a Similar Dose) Against Different Bacteria Strains (*S. aureus* ATCC 29213, *S. aureus* ATCC BAA-977, *P. aeruginosa* ATCC 27853 and *P. aeruginosa* ATCC 9721)

Samples	Moxi/Pir Disc	Moxi/Pir Fibers	Fus/Pir Disc	Fus/Pir Fibers
S. aureus ATCC 29213	40	31	40	31
S. aureus BAA 977	41	38	36	33
P. aeruginosa ATCC 27853	30	25	0.00	0.00
P. aeruginosa ATCC 9721	10	10	0.00	0.00

Abbreviations: Moxi, moxifloxacin; Fus, fusidic acid; Pir, pirfenidone.

P. aeruginosa using the zone of inhibition assay, which were recorded to be 32.33 ± 1.15 mm, 35.67 ± 1.53 mm, and 36.83 ± 2.56 mm, respectively. Liu et al[83] have also demonstrated an activity of Moxi loaded into PVA/CS nanofibers prepared at different ratios of both polymers. They have reported a zone of inhibition between 41 and 42 mm against *S. aureus* and between 8 and 31 mm against *P. aeruginosa*.

Fus/Pir coaxial nanofiber mat was also tested for its antibacterial activity against *S. aureus* and *P. aeruginosa*. The nanofibers and the positive control (discs) showed zones of inhibition of 31 mm and 40 mm, respectively, against *S. aureus* (ATCC 29213), and 33 mm and 36 mm, against *S. aureus* (ATCC BAA-977), as shown in Table 2. Both systems did not show any activity against the two strains of *P. aeruginosa*, which was expected due to the low Fus dose used in this study compared to the drug MIC (>512 µg/mL). The blank fibers did not report any antibacterial activity against both bacteria. This nanofiber system has also been proven to maintain the efficacy of Fus after being electrospun. Said et al[44] exhibited that Fus-incorporated PLGA nanofibers were able to inhibit pathogenic bacteria, with inhibition zones of 46.35 mm against *S. aureus* and 33.5 mm against *P. aeruginosa*. In addition, Gilchrist et al[84] have shown an antibacterial activity of combining Fus and rifampicin-loaded PLGA against four Gram-positive *Staphylococcus* bacterial strains. Supplementary Figures 4–8 show the zone of inhibitions of this current study's nanofiber systems.

Determination of the Inhibitory Concentration (IC) of the Pure Drugs

It is essential to determine the ideal concentrations of the drugs that can be applied in vitro without resulting in any cytotoxicity to the cultured cells to assess the biocompatibility of the dual drug-loaded nanofiber systems with the normal cells. Cultured skin fibroblasts (ie, HFF-1) were exposed to solutions of Pir, Moxi, and Fus and their combination for 24 hours to determine the IC_{20} and IC_{50}. 80% viability (represents the IC20) was considered the maximum accepted growth inhibition in this study. Figure 7 depicts the cell viability after 24-hour exposure to the drugs alone or in combination with Pir. In Figure 7A, Pir showed a cell viability of >90% with all tested concentrations up to 500 µg/mL. In contrast, based on the charts in (Figure 7B and C), Moxi and Fus exhibited ≥80% cell viability in concentrations below 250 µg/

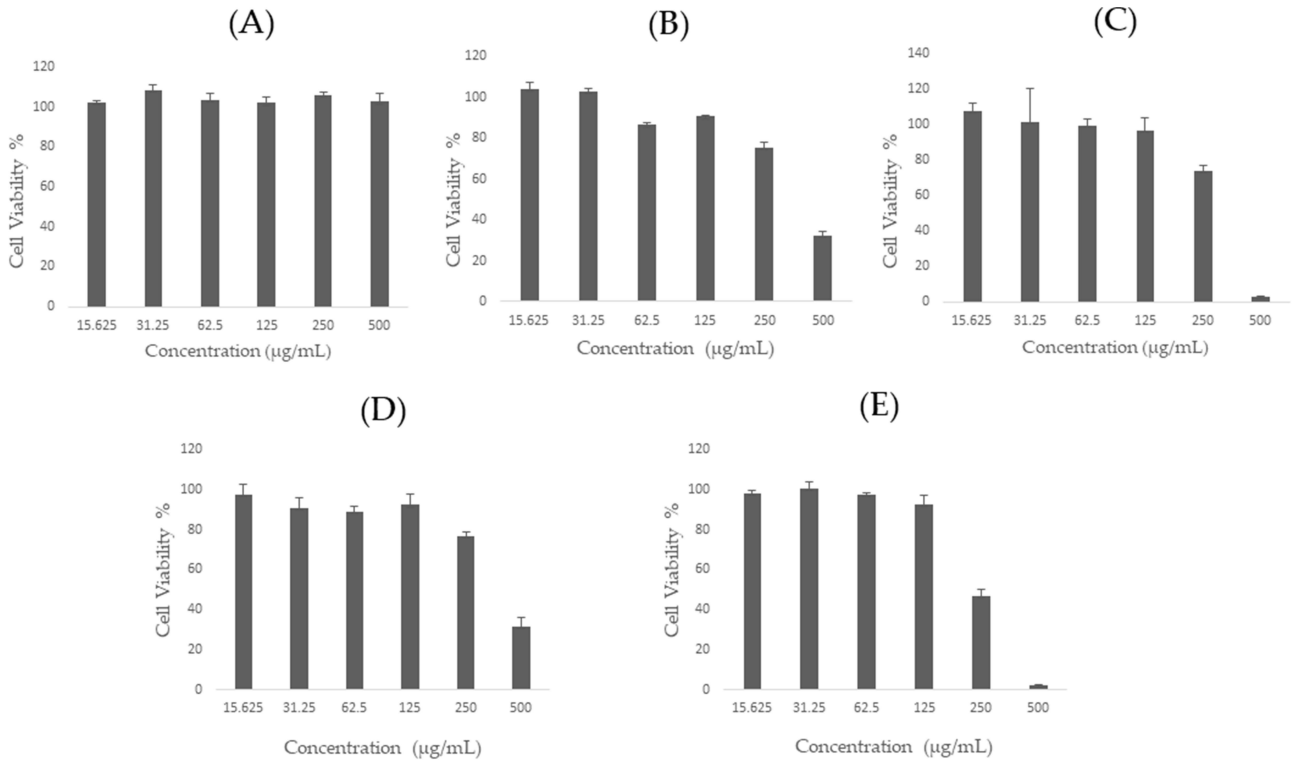

Figure 7 Cell viability % of (**A**), Pir; (**B**), Moxi; (**C**), Fus; (**D**), Moxi/Pir; and (**E**), Fus/Pir against HFF-1 cell line.
Notes: Results represent the average ± SD (n = 3).
Abbreviations: Moxi, moxifloxacin; Fus, fusidic acid; Pir, pirfenidone.

mL. A similar pattern was observed with both Moxi/Pir and Fus/Pir (charts in Figure 7D and E, respectively) indicating that the drugs have no interaction concerning the cell viability. Accordingly, a concentration of ≤150 µg/mL was selected for further biological experiments with the dual drug-loaded nanofiber systems.

In vivo Efficacy Testing of the Dual Drug-Loaded Nanofibers in Diabetic Wound Healing

A 14-day trial was conducted to determine whether the nanofibers loaded with either single or combinational therapies were effective in treating an induced wound in diabetic rats. The rats were administered with no treatments as a negative control, PVP-I dressing as a positive control, blank fibers, Moxi/Pir fibers, Fus/Pir fibers, Pir fibers, Moxi fibers, or Fus fibers once a day. The blank and the single drug-loaded fibers were tested as experimental controls. It is expected that the PVP drug-loaded nanofibers rapidly disintegrate upon contact with the wound site owing to the hydrophilic nature of the polymer and drugs. Consequently, it is necessary to change the nanofiber formulations daily. The size and status of the wound were monitored throughout the study. The rats' weight blood glucose and wound swabs were also collected to monitor the rats' health and to test the ability of dual drug-loaded nanofiber systems to prevent wound infection and the results are shown in the Supplementary Figures 9, 10 and 13, respectively. Overall, all treatment groups showed a reduction in the wound area over time, as demonstrated in Figure 8 and the Supplementary Figure 11, and representative images of the healing progression to 13 days are shown in Supplementary Figure 12.

Results indicated that on day 2, an initial reduction in the wound size was seen with PVP-I dressing, Fus fibers and Moxi fibers and no significant difference in the wound size between the three groups was apparent. There was, however, a significant reduction in the wound size between PVP-I dressing and Pir, Moxi/Pir and Fus/Pir fibers as well as the Fus fibers and Fus/Pir fibers (Figure 8, Supplementary Figures 11 and 12 and Supplementary Table 3). On day 4, the reduction in the wound size was more significant in animals treated with Fus fibers compared to the control, ie, PVP-I dressing, and fiber combinational therapy (Figure 8, Supplementary Figures 11 and 12 and Supplementary Table 3). Throughout day 6, the fibers with the combination therapy and the Fus-only fibers started to take the lead in wound closer with Fus/Pir fibers showing the most significant difference and a complete wound closer on day 8. All drug-loaded fibers were able to show a significant difference in the wound size on day 9 compared to PVP-I dressing and the blank fibers (Figure 8 and Supplementary Figures 11 and 12). Both single-loaded Fus and Moxi fibers showed complete wound closure on day 11. All other animal groups showed wounds closer on day 13 (Figure 8 and Supplementary Figures 11 and 12). No significant difference between animal weights was found between different treatment groups as shown in Supplementary Figure 9. In summary, although PVP-I dressing seemed to initiate wound healing earlier than other treatments, apparently Fus/Pir fibers were able to accelerate the wound healing and an almost complete wound closure earlier than the other systems. It is noteworthy that one animal in the control group died throughout treatment, most probably due to wound burden.

Overall, this study was conducted as a pilot study to investigate the potential of utilizing drug-loaded nanofiber dressings to accelerate wound healing in a diabetic wound model in rats. Specifically, the efficacy of these nanofibers, loaded with either antibiotics, anti-inflammatory agents, or a combination of both, was compared to commercially available dressings, ie, INADINE, in expediting the wound healing process. As previously mentioned, among the various tested systems, the Fus/Pir fibers exhibited the ability to accelerate wound healing, resulting in nearly complete closure of the wound at an earlier stage compared to the other systems. Following this, the nanofiber systems that are loaded with the antibiotics, namely Fus nanofibers, Moxi nanofibers, and the combination of Moxi/Pir nanofibers, showed promising results. However, it is important to note that this study had a limitation in terms of evaluating their abilities to prevent an induced infection, such as *S. aureus*-induced infection that commonly occurs in diabetic foot ulcer patients, and to suppress inflammation in diabetic rats. This was due to the restrictions in the animal facility to use pathogens and to distress the rats by triggering an inflammatory response. Instead, the rats were housed in cages under uncontrolled conditions, which potentially contributed to infections, as shown in the calculated number of microbial colonies on days 1, 3, 5, 7, 9, 11 and 13 (Supplementary Figure 13). The total number of colonies was determined for each swab collected from different formulation treatments. It is also important to acknowledge that this study did not identify the type of specific bacterial strains, which can be considered as another limitation. Furthermore, there was a variability observed in

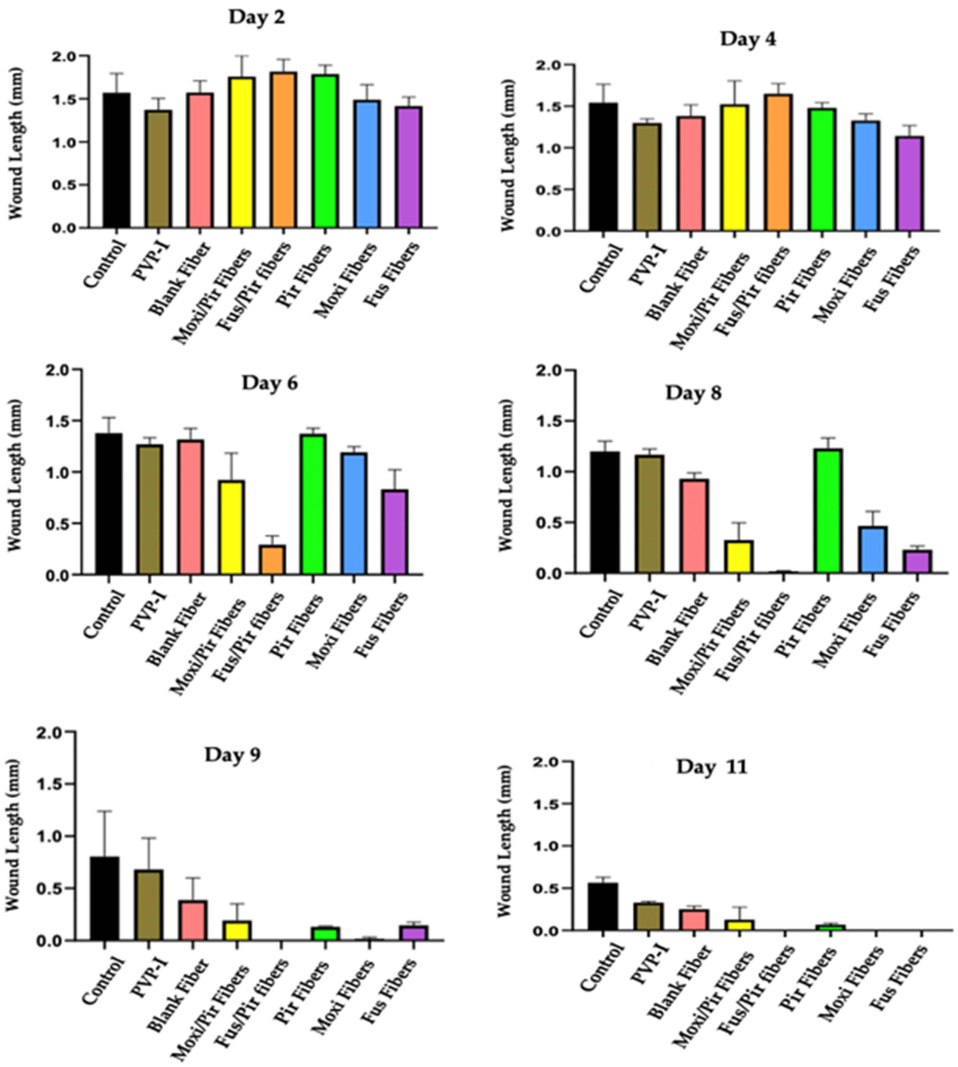

Figure 8 Representation of daily wound size treated with drug-loaded fibers in comparison with Control non-treated, positive control, and blank fibers.
Notes: Data are represented as average ± SD (n = 4).
Abbreviations: Moxi, moxifloxacin; Fus, fusidic acid; Pir, pirfenidone.

the number of colonies both daily and among different rats, even among those treated with the same formulation. Therefore, we recommend conducting further investigation under more controlled conditions, including aseptic housing of the rats being tested, and specifically inducing pathogenic bacterial infection and inflammation in the diabetic rats. This will help to provide more precise and accurate insight into the potential effectiveness of the tested dual drug-loaded nanofiber systems.

Compared to previous studies, it was reported that utilizing nanofibers with or without drugs is effective in enhancing wound healing in animal models including eye, skin, and diabetic foot wounds.[36,85,86] In line with these findings, our study aimed to investigate the potential of an antibiotic and an anti-inflammatory drug combined loaded into electrospun nanofibers of PVP in wound healing treatment, ie, diabetic wounds in rats. In a similar study, Hameed et al[49] loaded moxifloxacin into CS and PEO nanofibers and demonstrated its antibacterial properties both in vitro and in vivo. In addition, they observed a faster wound closure in injured rats with a 1 cm^2 wound area compared to the untreated and blank groups. This rapid wound healing might be linked to the use of CS, which is known for its antibacterial and anti-inflammatory properties.[87,88] In a porcine model, Mayandi et al[85] showed the efficacy of superhydrophilic electrospun gelatin nanofiber dressings (NFDs) containing the antimicrobial polymer polylysine (PL), crosslinked by polydopamine (pDA), for eradicating the bacterial bioburden and

promoting wound healing in critically colonized wounds with second-degree burns. Different compositions and structures of nanofiber dressings have the potential to treat a variety of wound types, as highlighted in this study.

The coaxial electrospinning technology represents another promising way to make fibrous wound dressings with a customizable core-shell structure. As a result of this technique, dressings can be formulated with distinct functionalities and are more versatile and effective.[89] Samadian et al[17] fabricated Cellulose Acetate/Gelatin (CA/Gel) electrospun mats loaded with berberine (Beri) for diabetic foot ulcer treatment. Streptozotocin-induced diabetic rats were used to evaluate the wound-healing efficacy of these dressings. In this study, nanofiber dressings were demonstrated to be effective in treating specific wound types, including DFUs. Another study has also shown that the PLGA nanofibers loaded with metformin can be effective in the treatment of diabetic wounds by Lee et al.[86] They exhibited the ability of metformin as an accelerator in the early stages of wound healing in diabetic rats, which highlights its active role in treating diabetic wounds. In recent developments, Yu et al have combined sulfated chitosan (SCS) with polydopamine-gentamicin (PDA-GS) and modified them onto porous poly(L-lactic acid) (PLA) nanofibers. This innovative approach aims to create multifunctional antibacterial (GS) agents against Staphylococcus aureus, along with immunomodulatory and angiogenic properties to enhance the overall diabetic wound-healing process for patients.[90]

These studies collectively indicated that nanofiber-based wound dressings are effective in delivering different types of drugs, enhancing wound closure, and promoting wound healing in animal models. To maximize the therapeutic potential of nanofiber dressings for various wound types, including diabetic foot ulcers, it is essential to select appropriate materials, implement drug-loading strategies, and take wound-specific considerations into account.

Histopathological Assessment of the Wounds

Microscopic histopathological examination of H&E stained representative tissue sections obtained from the eight groups of animals on different days is shown in Figure 9. The results demonstrated the following: Group 1 (control), healing of the wound in sections taken after day 11 in all samples. Group 2 (PVP-I dressing), healing of the wound in sections taken

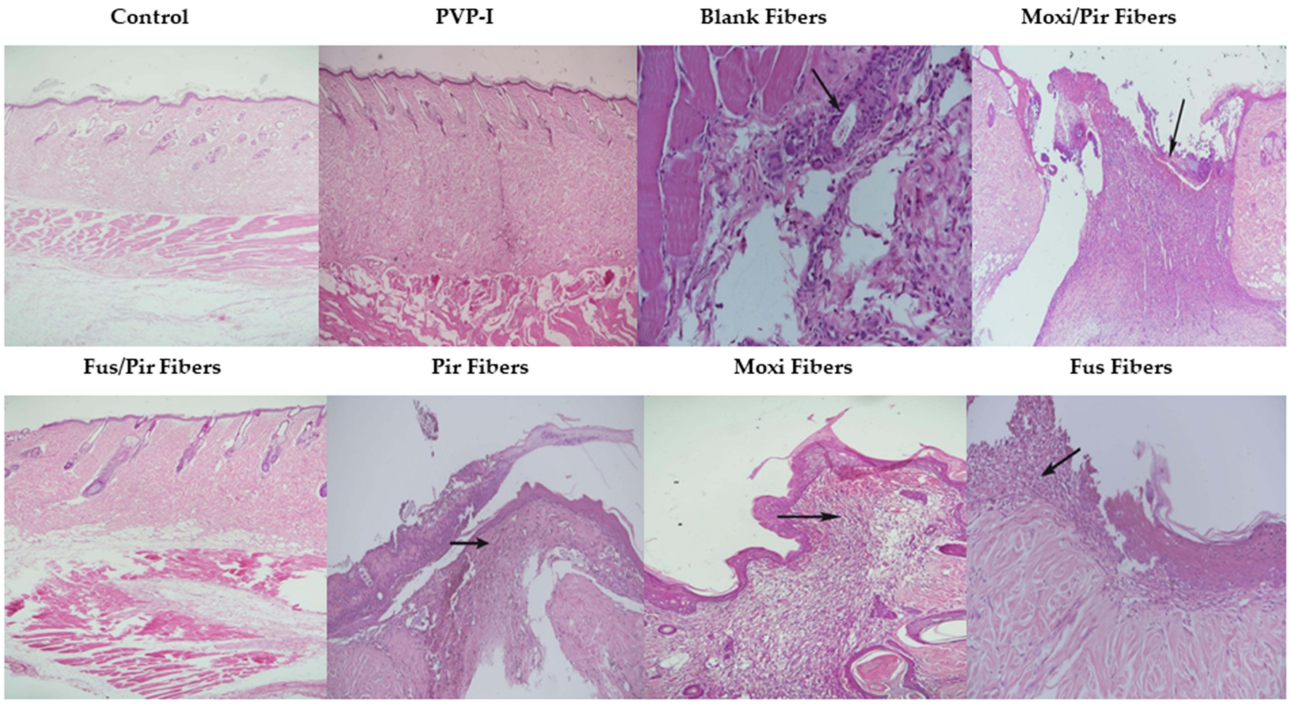

Figure 9 Photomicrographs of tissue sections taken from the skin of rats showing features of the healed wound in the Control group, PVP-I and Fus/Pir fibers (H&E stain, lens magnification of X4), Pir fibers and Moxi fibers (H&E stain, lens magnification of X10), Blank fibers and Fus fibers (H&E stain, lens magnification of X20), Moxi/Pir fibers (H&E stain, lens magnification of X40).
Notes: Focal foreign body giant cell reactions are shown in two rats from the Blank fiber-treated group (black arrow), ulcerating wounds with granulation tissue are shown in one rat treated with Moxi/Pir fibers (black arrow) and a small focus of granulation tissue in one rat treated with Pir fibers, Mox fibers and Fus fibers (black arrow).
Abbreviations: H&E, hematoxylin and eosin staining; Moxi, moxifloxacin; Fus, fusidic acid; Pir, pirfenidone.

after day 11 in all samples. Group 3 (blank fibre), healing of the wound in sections taken after day 11 in all samples, however, two of them showed focal foreign body reactions. Group 4 (Moxi/Pir fibres), healing of the wound in sections taken after day 11 in two-thirds of the samples. One-third showed wound ulcers with an underlying large amount of granulation tissue. Group 5 (Fus/Pir fibers), healing of the wound in sections taken on day 8 in two-thirds of the samples. One-third showed wound ulcers with underlying focal granulation tissue. Group 6 (Pir fibers), healing of the wound in sections taken on day 11 in two-thirds of the samples. One-third showed a small wound ulcer with underlying focal granulation tissue. Group 7 (Moxi fibers), healing of the wound in sections taken on day 8 in two-thirds of the samples. One-third showed a small amount of granulation tissue. Group 8 (Fus fibers), healing of the wound in sections taken on day 11 in two-thirds of the samples. One-third showed a small wound ulcer with a small amount of granulation tissue. None of the samples showed significant scarring. In summary, wound healing was fastest in Group 5 (Fus/Pir fibers) followed by Group 7 (Moxi fiber), Group 6 (Pir fiber) and Group 8 (Fus fibers), in two-thirds of the groups' samples. Wound healing took a longer time in the other groups, ie, Group 1 (control), Group 2 (PVP-I dressing), Group 3 (blank fiber) and Group 4 (Moxi/Pir fiber).

Conclusion

Diabetic foot ulcers have become one of the most common and severe complications of diabetes mellitus, resulting in significant morbidity and mortality. The development of a dual drug-loaded coaxial nanofiber dressing holds promise for accelerating the wound healing process in diabetic foot ulcers. This study successfully fabricated bioactive PVP nanofibers loaded with a combination of an antibiotic and an anti-inflammatory drug using an electrospinning technique and the efficacy of the dual drug-loaded nanofiber systems was evaluated through in vitro and in vivo studies. The results demonstrated that the fibers had a smooth surface with bead-less and pore-less surfaces. The nanofibers also exhibited a relatively high EE% of the drugs, and within 24 hours, the release of the drugs was 100% for Moxi and Pir, while Fus and Pir were released at 65% and 80%, respectively, at the same time frame. Furthermore, the cytotoxicity assessment indicated that the safety of the drugs at a selected concentration of ≤150 µg/mL to be used for further biological assessments. For the microbiological assessment, both dual drug-loaded nanofibers showed potent antibacterial activity against various pathogenic strains, with the Moxi being more sensitive to both the Gram-positive *S. aureus* and the Gram-negative *P. aeruginosa*. In the in vivo diabetic rat model, all tested formulations promoted a faster wound closure compared to the control groups, indicating their potential for accelerating wound healing. Notably, the combination of Fus and Pir nanofibers exhibited the most remarkable results, achieving wound healing in 8 days compared to the control groups.

Overall, our findings suggest that the developed dual drug-loaded nanofiber dressings have a potential therapeutic approach for diabetic foot ulcers in terms of accelerating wound closure. Based on the findings of this study, it is advisable to pursue a further investigation. This includes implementing aseptic housing for the rats involved in the study and deliberately inducing pathogenic bacterial infection and inflammation in diabetic rats. Conducting specific anti-inflammatory tests targeting a diabetic rat model would provide valuable insights into the potential benefits of these nanofibers in managing inflammation in such conditions. By doing so, more precise and accurate insights can be obtained regarding the potential effects of the loaded drugs to treat the infection and suppress the inflammation. Moreover, the mechanical properties of coaxial PVP nanofibers should be assessed to determine their suitability for wound healing applications. These additional measures will contribute to a more comprehensive understanding of the efficacy and safety of the dual drug-loaded nanofiber dressings, allowing a better understanding of their potential clinical applications.

Institutional Review Board Statement

This animal study was performed in controlled facilities in compliance with protocol number KSU-SE-22-5 approved by the Research Ethics Committee at King Saud University (KSU).

Data Sharing Statement

The authors confirm that the data supporting the findings of this study are available within the article.

Acknowledgments

The authors want to thank Dr Rawan Fitaihi (College of Pharmacy, King Saud University, Riyadh, Saudi Arabia) and Ms Bayan Alshehri (Health Sector, King Abdulaziz City for Science and Technology, Riyadh, Saudi Arabia) for their contributions in this study.

Author Contributions

All authors made a significant contribution to the work reported, whether that is in the conception, study design, execution, acquisition of data, analysis and interpretation, or in all these areas; took part in drafting, revising or critically reviewing the article; gave final approval of the version to be published; have agreed on the journal to which the article has been submitted; and agree to be accountable for all aspects of the work.

Funding

This work was funded by the National Industrial Development and Logistics Program (NIDLP) through the Health Initiative and the Technology Leader Program Initiative, project numbers 20–0103 and 20–0051.

Disclosure

The authors declare that they have no financial or non-financial conflicts of interest.

References

1. Sorber R, Abularrage CJ. Diabetic foot ulcers: epidemiology and the role of multidisciplinary care teams. *Semin Vasc Surg*. 2021;34(1):47–53. doi:10.1053/j.semvascsurg.2021.02.006
2. Xia D, Liu Y, Cao W, et al. Dual-functional nanofibrous patches for accelerating wound healing. *Int J Mol Sci*. 2022;23(18). doi:10.3390/ijms231810983
3. Falanga V. Wound healing and its impairment in the diabetic foot. *Lancet Lond Engl*. 2005;366(9498):1736–1743. doi:10.1016/S0140-6736(05)67700-8
4. Dasari N, Jiang A, Skochdopole A, et al. Updates in diabetic wound healing, inflammation, and scarring. *Semin Plast Surg*. 2021;35(3):153–158. doi:10.1055/s-0041-1731460
5. Liu X, Xu H, Zhang M, Yu DG. Electrospun medicated nanofibers for wound healing: review. *Membranes*. 2021;11(10):770. doi:10.3390/membranes11100770
6. Macdonald KE, Jordan CY, Crichton E, et al. A retrospective analysis of the microbiology of diabetic foot infections at a Scottish tertiary hospital. *BMC Infect Dis*. 2020;20(1):218. doi:10.1186/s12879-020-4923-1
7. Radzieta M, Sadeghpour-Heravi F, Peters TJ, et al. A multiomics approach to identify host-microbe alterations associated with infection severity in diabetic foot infections: a pilot study. *Npj Biofilms Microbiomes*. 2021;7(1):29. doi:10.1038/s41522-021-00202-x
8. Janka-Zires M, Almeda-Valdes P, Uribe-Wiechers AC, et al. Topical administration of pirfenidone increases healing of chronic diabetic foot ulcers: a randomized crossover study. *J Diabetes Res*. 2016;2016:7340641. doi:10.1155/2016/7340641
9. Dreifke MB, Jayasuriya AA, Jayasuriya AC. Current wound healing procedures and potential care. *Mater Sci Eng C Mater Biol Appl*. 2015;48:651–662. doi:10.1016/j.msec.2014.12.068
10. Han G, Ceilley R. Chronic wound healing: a review of current management and treatments. *Adv Ther*. 2017;34(3):599–610. doi:10.1007/s12325-017-0478-y
11. Dumville JC, Lipsky BA, Hoey C, Cruciani M, Fiscon M, Xia J. Topical antimicrobial agents for treating foot ulcers in people with diabetes. *Cochrane Database Syst Rev*. 2017;6(6):CD011038. doi:10.1002/14651858.CD011038.pub2
12. Liu H, Li Z, Zhao Y, et al. Novel diabetic foot wound dressing based on multifunctional hydrogels with extensive temperature-tolerant, durable, adhesive, and intrinsic antibacterial properties. *ACS Appl Mater Interf*. 2021;13(23):26770–26781. doi:10.1021/acsami.1c05514
13. Korupalli C, Li H, Nguyen N, et al. Conductive materials for healing wounds: their incorporation in electroactive wound dressings, characterization, and perspectives. *Adv Healthc Mater*. 2021;10(6):e2001384. doi:10.1002/adhm.202001384
14. Broussard KC, Powers JG. Wound dressings: selecting the most appropriate type. *Am J Clin Dermatol*. 2013;14(6):449–459. doi:10.1007/s40257-013-0046-4
15. Moura LIF, Dias AMA, Carvalho E, de Sousa HC. Recent advances on the development of wound dressings for diabetic foot ulcer treatment--a review. *Acta Biomater*. 2013;9(7):7093–7114. doi:10.1016/j.actbio.2013.03.033
16. Wei S, You Y, Ma Y, et al. Bi-layer supramolecular polydimethylsiloxane elastomer film: synthesis, characterization, and application in wound dressing on normal and diabetic rat. *React Funct Polym*. 2019;141:21–32. doi:10.1016/j.reactfunctpolym.2019.05.002
17. Samadian H, Zamiri S, Ehterami A, et al. Electrospun cellulose acetate/gelatin nanofibrous wound dressing containing berberine for diabetic foot ulcer healing: in vitro and in vivo studies. *Sci Rep*. 2020;10(1):8312. doi:10.1038/s41598-020-65268-7
18. Sun Y, Cheng S, Lu W, Wang Y, Zhang P, Yao Q. Electrospun fibers and their application in drug controlled release, biological dressings, tissue repair, and enzyme immobilization. *RSC Adv*. 2019;9(44):25712–25729. doi:10.1039/c9ra05012d
19. Nikmaram N, Roohinejad S, Hashemi S, et al. Emulsion-based systems for fabrication of electrospun nanofibers: food, pharmaceutical and biomedical applications. *RSC Adv*. 2017;7(46):28951–28964. doi:10.1039/C7RA00179G

20. Memic A, Abdullah T, Mohammed HS, Joshi Navare K, Colombani T, Bencherif SA. Latest progress in electrospun nanofibers for wound healing applications. *ACS Appl Bio Mater*. 2019;2(3):952–969. doi:10.1021/acsabm.8b00637
21. Sun M, Chen S, Ling P, Ma J, Wu S. Electrospun methacrylated gelatin/poly(L-Lactic Acid) nanofibrous hydrogel scaffolds for potential wound dressing application. *Nanomaterials*. 2022;12(1). doi:10.3390/nano12010006
22. Ali IH, Khalil IA, El-Sherbiny IM. Single-Dose electrospun nanoparticles-in-nanofibers wound dressings with enhanced epithelialization, collagen deposition, and granulation properties. *ACS Appl Mater Interf*. 2016;8(23):14453–14469. doi:10.1021/acsami.6b04369
23. Goyal R, Macri LK, Kaplan HM, Kohn J. Nanoparticles and nanofibers for topical drug delivery. *J Control Release off J Control Release Soc*. 2016;240:77–92. doi:10.1016/j.jconrel.2015.10.049
24. Franco P, De Marco I. The use of poly(N-vinyl pyrrolidone) in the delivery of drugs: a review. *Polymers*. 2020;12(5). doi:10.3390/polym12051114
25. Rasekh M, Karavasili C, Soong YL, et al. Electrospun PVP-indomethacin constituents for transdermal dressings and drug delivery devices. *Int J Pharm*. 2014;473(1–2):95–104. doi:10.1016/j.ijpharm.2014.06.059
26. Koczkur KM, Mourdikoudis S, Polavarapu L, Skrabalak SE. Polyvinylpyrrolidone (PVP) in nanoparticle synthesis. *Dalton Trans Camb Engl*. 2015;44(41):17883–17905. doi:10.1039/c5dt02964c
27. Yu DG, Zhang XF, Shen XX, Brandford-White C, Zhu LM. Ultrafine ibuprofen-loaded polyvinylpyrrolidone fiber mats using electrospinning. *Polym Int*. 2009;58(9):1010–1013. doi:10.1002/pi.2629
28. Rahmani F, Ziyadi H, Baghali M, Luo H, Ramakrishna S. Electrospun PVP/PVA Nanofiber Mat as a Novel Potential Transdermal Drug-Delivery System for Buprenorphine: a Solution Needed for Pain Management. *Appl Sci*. 2021;11(6). doi:10.3390/app11062779
29. Huang S, Zhou L, Li MC, Wu Q, Kojima Y, Zhou D. Preparation and properties of electrospun poly (Vinyl Pyrrolidone)/cellulose nanocrystal/silver nanoparticle composite fibers. *Mater Basel Switz*. 2016;9(7). doi:10.3390/ma9070523
30. Zhang C, Yang X, Yu L, et al. Electrospun polyasparthydrazide nanofibrous hydrogel loading with in-situ synthesized silver nanoparticles for full-thickness skin wound healing application. *Mater Des*. 2024;239:112818. doi:10.1016/j.matdes.2024.112818
31. Li Y, Zhao W, Chen S, Zhai H, Wu S. Bioactive electrospun nanoyarn-constructed textile dressing patches delivering Chinese herbal compound for accelerated diabetic wound healing. *Mater Des*. 2024;237:112623. doi:10.1016/j.matdes.2023.112623
32. Singh B, Dhiman A. Designing bio-mimetic moxifloxacin loaded hydrogel wound dressing to improve antioxidant and pharmacology properties. *RSC Adv*. 2015;5. doi:10.1039/C5RA06857F
33. Jacobsen F, Fisahn C, Sorkin M, et al. Efficacy of topically delivered moxifloxacin against wound infection by Pseudomonas aeruginosa and methicillin-resistant Staphylococcus aureus. *Antimicrob Agents Chemother*. 2011;55(5):2325–2334. doi:10.1128/AAC.01071-10
34. MacGowan AP, Rogers CA, Holt HA, Bowker KE. Activities of moxifloxacin against, and emergence of resistance in, Streptococcus pneumoniae and Pseudomonas aeruginosa in an in vitro pharmacokinetic model. *Antimicrob Agents Chemother*. 2003;47(3):1088–1095. doi:10.1128/AAC.47.3.1088-1095.2003
35. Lipsky BA, Hoey C. Topical antimicrobial therapy for treating chronic wounds. *Clin Infect Dis off Publ Infect Dis Soc Am*. 2009;49(10):1541–1549. doi:10.1086/644732
36. Tawfik EA, Alshamsan A, Abul Kalam M, et al. In vitro and in vivo biological assessment of dual drug-loaded coaxial nanofibers for the treatment of corneal abrasion. *Int J Pharm*. 2021;604:120732. doi:10.1016/j.ijpharm.2021.120732
37. Gasca-Lozano LE, Lucano-Landeros S, Ruiz-Mercado H, et al. Pirfenidone accelerates wound healing in chronic diabetic foot ulcers: a randomized, double-blind controlled trial. *J Diabetes Res*. 2017;2017:3159798. doi:10.1155/2017/3159798
38. Mitani Y, Sato K, Muramoto Y, et al. Superoxide scavenging activity of pirfenidone–iron complex. *Biochem Biophys Res Commun*. 2008;372(1):19–23. doi:10.1016/j.bbrc.2008.04.093
39. Zurkova M, Kriegova E, Kolek V, et al. Effect of pirfenidone on lung function decline and survival: 5-yr experience from a real-life IPF cohort from the Czech EMPIRE registry. *Respir Res*. 2019;20(1):16. doi:10.1186/s12931-019-0977-2
40. Song MJ, Moon SW, Choi JS, et al. Efficacy of low dose pirfenidone in idiopathic pulmonary fibrosis: real world experience from a tertiary university hospital. *Sci Rep*. 2020;10(1):21218. doi:10.1038/s41598-020-77837-x
41. Evani SJ, Karna SLR, Seshu J, Leung KP. Pirfenidone regulates LPS mediated activation of neutrophils. *Sci Rep*. 2020;10(1):19936. doi:10.1038/s41598-020-76271-3
42. Pan J, Liu N, Sun H, Xu F. Preparation and characterization of electrospun PLCL/Poloxamer nanofibers and dextran/gelatin hydrogels for skin tissue engineering. *PLoS One*. 2014;9(11):e112885. doi:10.1371/journal.pone.0112885
43. Kim K, Luu YK, Chang C, et al. Incorporation and controlled release of a hydrophilic antibiotic using poly(lactide-co-glycolide)-based electrospun nanofibrous scaffolds. *J Control Release off J Control Release Soc*. 2004;98(1):47–56. doi:10.1016/j.jconrel.2004.04.009
44. Said SS, Aloufy AK, El-Halfawy OM, Boraei NA, El-Khordagui LK. Antimicrobial PLGA ultrafine fibers: interaction with wound bacteria. *Eur J Pharm Biopharm Off J Arbeitsgemeinschaft Pharm Verfahrenstechnik EV*. 2011;79(1):108–118. doi:10.1016/j.ejpb.2011.03.002
45. Wang L, Yang J, Ran B, et al. Small molecular TGF-β1-inhibitor-loaded electrospun fibrous scaffolds for preventing hypertrophic scars. *ACS Appl Mater Interf*. 2017;9(38):32545–32553. doi:10.1021/acsami.7b09796
46. Razzaq A, Khan ZU, Saeed A, et al. Development of cephradine-loaded gelatin/polyvinyl alcohol electrospun nanofibers for effective diabetic wound healing: in-vitro and in-vivo assessments. *Pharmaceutics*. 2021;13(3). doi:10.3390/pharmaceutics13030349
47. Iqbal H, Khan BA, Khan ZU, et al. Fabrication, physical characterizations and in vitro antibacterial activity of cefadroxil-loaded chitosan/poly (vinyl alcohol) nanofibers against Staphylococcus aureus clinical isolates. *Int J Biol Macromol*. 2020;144:921–931. doi:10.1016/j.ijbiomac.2019.09.169
48. Kamal R, Razzaq A, Ali Shah K, et al. Evaluation of cephalexin-loaded PHBV nanofibers for MRSA-infected diabetic foot ulcers treatment. *J Drug Deliv Sci Technol*. 2022;71:103349. doi:10.1016/j.jddst.2022.103349
49. Hameed M, Rasul A, Nazir A, et al. Moxifloxacin-loaded electrospun polymeric composite nanofibers-based wound dressing for enhanced antibacterial activity and healing efficacy. *Int J Polym Mater Polym Biomater*. 2021;70(17):1271–1279. doi:10.1080/00914037.2020.1785464
50. Tottoli EM, Benedetti L, Riva F, et al. Electrospun fibers loaded with pirfenidone: an innovative approach for scar modulation in complex wounds. *Polymers*. 2023;15(20). doi:10.3390/polym15204045
51. Alkahtani ME, Aodah AH, Abu Asab OA, Basit AW, Orlu M, Tawfik EA. Fabrication and characterization of fast-dissolving films containing escitalopram/quetiapine for the treatment of major depressive disorder. *Pharmaceutics*. 2021;13(6). doi:10.3390/pharmaceutics13060891

52. Alshaya HA, Alfahad AJ, Alsulaihem FM, et al. Fast dissolving nifedipine and atorvastatin calcium electrospun nanofibers as a potential buccal delivery system. *Pharmaceutics*. 2022;14(2). doi:10.3390/pharmaceutics14020358
53. Almuwallad SS, Alzahrani DA, Aburayan WS, et al. Eflornithine hydrochloride-loaded electrospun nanofibers as a potential face mask for hirsutism application. *Pharmaceutics*. 2023;15(9). doi:10.3390/pharmaceutics15092343
54. Gareth R, Williams, Bahijja T, Raimi-Abraham CJ. *Nanofibres in Drug Delivery*. UCL Press; 2018.
55. Alamer AA, Alsaleh NB, Aodah AH, et al. Development of imeglimin electrospun nanofibers as a potential buccal antidiabetic therapeutic approach. *Pharmaceutics*. 2023;15(4). doi:10.3390/pharmaceutics15041208
56. Wang Y, Liu Y, Qian Y, Lv L, Li X, Liu Y. Characteristics of MgO/PCL/PVP antibacterial nanofiber membranes produced by electrospinning technology. *Surf Interfaces*. 2022;28:101661. doi:10.1016/j.surfin.2021.101661
57. Shah A, Ali Buabeid M, Arafa ESA, Hussain I, Li L, Murtaza G. The wound healing and antibacterial potential of triple-component nanocomposite (chitosan-silver-sericin) films loaded with moxifloxacin. *Int J Pharm*. 2019;564:22–38. doi:10.1016/j.ijpharm.2019.04.046
58. Malani M, Thodikayil AT, Saha S, Nirmal J. Carboxylated nanofibrillated cellulose empowers moxifloxacin to overcome Staphylococcus aureus biofilm in bacterial keratitis. *Carbohydr Polym*. 2024;324:121558. doi:10.1016/j.carbpol.2023.121558
59. Tawfik EA, Craig DQM, Barker SA. Dual drug-loaded coaxial nanofibers for the treatment of corneal abrasion. *Int J Pharm*. 2020;581:119296. doi:10.1016/j.ijpharm.2020.119296
60. Kulshrestha R, Singh A, Kumar P, et al. Nanoapproach targeting TGFβ1-Smad pathway and modulating lung microenvironment. *Process Biochem*. 2022;121:126–141. doi:10.1016/j.procbio.2022.06.027
61. Marian E, Tita B, Duteanu N, et al. Antimicrobial activity of fusidic acid inclusion complexes. *Int J Infect Dis*. 2020;101:65–73. doi:10.1016/j.ijid.2020.09.1465
62. Aburayan WS, Booq RY, BinSaleh NS, et al. The Delivery of the novel drug "halicin" using electrospun fibers for the treatment of pressure ulcer against pathogenic bacteria. *Pharmaceutics*. 2020;12(12). doi:10.3390/pharmaceutics12121189
63. Gültekin Y, Korkmaz Ç, Öztürk N, et al. Preparation and evaluation of fast-dissolving albendazole sulfoxide and praziquantel-loaded polyvinyl-pyrrolidone nanofiber films by electrospinning. *J Drug Deliv Sci Technol*. 2024;92:105304. doi:10.1016/j.jddst.2023.105304
64. Borhade DD, Nangare SN, Patil DA, Patil PO, Patil GS, Patil GB. Preparation of pirfenidone loaded chitosan-polyvinyl alcohol-graphene oxide-based scaffold: spectroscopical characterizations and antibacterial activity. *J Drug Deliv Sci Technol*. 2023;82:104325. doi:10.1016/j.jddst.2023.104325
65. Shah A, Ashames AA, Buabeid MA, Murtaza G. Synthesis, in vitro characterization and antibacterial efficacy of moxifloxacin-loaded chitosan-pullulan-silver-nanocomposite films. *J Drug Deliv Sci Technol*. 2020;55:101366. doi:10.1016/j.jddst.2019.101366
66. Thakur K, Sharma G, Singh B, Chhibber S, Patil AB, Katare OP. Chitosan-tailored lipidic nanoconstructs of Fusidic acid as promising vehicle for wound infections: an explorative study. *Int J Biol Macromol*. 2018;115:1012–1025. doi:10.1016/j.ijbiomac.2018.04.092
67. Gilchrist SE, Rickard DL, Letchford K, Needham D, Burt HM. Phase separation behavior of fusidic acid and rifampicin in PLGA microspheres. *Mol Pharm*. 2012;9(5):1489–1501. doi:10.1021/mp300099f
68. Huo P, Han X, Zhang W, Zhang J, Kumar P, Liu B. Electrospun nanofibers of polycaprolactone/collagen as a sustained-release drug delivery system for artemisinin. *Pharmaceutics*. 2021;13(8). doi:10.3390/pharmaceutics13081228
69. Liang Q, Gao Q. Effect of amylose content on the preparation for carboxymethyl starch/pullulan electrospun nanofibers and their properties as encapsulants of thymol. *Food Hydrocoll*. 2023;136:108250. doi:10.1016/j.foodhyd.2022.108250
70. Bai Y, Wang D, Zhang Z, et al. Testing of fast dissolution of ibuprofen from its electrospun hydrophilic polymer nanocomposites. *Polym Test*. 2021;93:106872. doi:10.1016/j.polymertesting.2020.106872
71. Almostafa MM, Elsewedy HS, Shehata TM, Soliman WE. Novel formulation of fusidic acid incorporated into a myrrh-oil-based nanoemulgel for the enhancement of skin bacterial infection treatment. *Gels Basel Switz*. 2022;8(4). doi:10.3390/gels8040245
72. Leaper D, Assadian O, Edmiston CE. Approach to chronic wound infections. *Br J Dermatol*. 2015;173(2):351–358. doi:10.1111/bjd.13677
73. Abid HMU, Hanif M, Mahmood K, Aziz M, Abbas G, Latif H. Wound-healing and antibacterial activity of the quercetin–4-formyl phenyl boronic acid complex against bacterial pathogens of diabetic foot ulcer. *ACS Omega*. 2022;7(28):24415–24422. doi:10.1021/acsomega.2c01819
74. Kalan LR, Meisel JS, Loesche MA, et al. Strain- and species-level variation in the microbiome of diabetic wounds is associated with clinical outcomes and therapeutic efficacy. *Cell Host Microbe*. 2019;25(5):641–655.e5. doi:10.1016/j.chom.2019.03.006
75. Speciale A, Musumeci R, Blandino G, Milazzo I, Caccamo F, Nicoletti G. Minimal inhibitory concentrations and time-kill determination of moxifloxacin against aerobic and anaerobic isolates. *Int J Antimicrob Agents*. 2002;19(2):111–118. doi:10.1016/s0924-8579(01)00486-1
76. Masadeh MM, Alzoubi KH, Ahmed WS, Magaji AS. In vitro comparison of antibacterial and antibiofilm activities of selected fluoroquinolones against pseudomonas aeruginosa and methicillin-resistant Staphylococcus aureus. *Pathog Basel Switz*. 2019;8(1). doi:10.3390/pathogens8010012
77. Jones RN, Castanheira M, Rhomberg PR, Woosley LN, Pfaller MA. Performance of fusidic acid (CEM-102) susceptibility testing reagents: broth microdilution, disk diffusion, and Etest methods as applied to Staphylococcus aureus. *J Clin Microbiol*. 2010;48(3):972–976. doi:10.1128/JCM.01829-09
78. Coutant C, Olden D, Bell J, Turnidge JD. Disk diffusion interpretive criteria for fusidic acid susceptibility testing of staphylococci by the national committee for clinical laboratory standards method. *Diagn Microbiol Infect Dis*. 1996;25(1):9–13. doi:10.1016/0732-8893(96)00070-3
79. Howden BP, Grayson ML. Dumb and dumber--The potential waste of a useful antistaphylococcal agent: emerging fusidic acid resistance in Staphylococcus aureus. *Clin Infect Dis off Publ Infect Dis Soc Am*. 2006;42(3):394–400. doi:10.1086/499365
80. Skov R, Frimodt-Møller N, Espersen F. Correlation of MIC methods and tentative interpretive criteria for disk diffusion susceptibility testing using NCCLS methodology for fusidic acid. *Diagn Microbiol Infect Dis*. 2001;40(3):111–116. doi:10.1016/s0732-8893(01)00262-0
81. McGhee P, Clark C, Credito K, et al. In vitro activity of fusidic acid (CEM-102, sodium fusidate) against Staphylococcus aureus isolates from cystic fibrosis patients and its effect on the activities of tobramycin and amikacin against Pseudomonas aeruginosa and Burkholderia cepacia. *Antimicrob Agents Chemother*. 2011;55(5):2417–2419. doi:10.1128/AAC.01672-10
82. O'Brien TJ, Figueroa W, Welch M. Decreased efficacy of antimicrobial agents in a polymicrobial environment. *ISME J*. 2022;16(7):1694–1704. doi:10.1038/s41396-022-01218-7
83. Liu Q, Ouyang WC, Zhou XH, Jin T, Wu ZW. Antibacterial Activity and drug loading of moxifloxacin-Loaded Poly(Vinyl Alcohol)/chitosan electrospun nanofibers. *Front Mater*. 2021;3:8.
84. Gilchrist SE, Lange D, Letchford K, Bach H, Fazli L, Burt HM. Fusidic acid and rifampicin co-loaded PLGA nanofibers for the prevention of orthopedic implant associated infections. *J Control Release*. 2013;170(1):64–73. doi:10.1016/j.jconrel.2013.04.012

85. Mayandi V, Wen Choong AC, Dhand C, et al. Multifunctional antimicrobial nanofiber dressings containing ε-polylysine for the eradication of bacterial bioburden and promotion of wound healing in critically colonized wounds. *ACS Appl Mater Interf*. 2020;12(14):15989–16005. doi:10.1021/acsami.9b21683
86. Lee CH, Hsieh MJ, Chang SH, et al. Enhancement of diabetic wound repair using biodegradable nanofibrous metformin-eluting membranes: in vitro and in vivo. *ACS Appl Mater Interf*. 2014;6(6):3979–3986. doi:10.1021/am405329g
87. Croisier F, Sibret P, DuPont-Gillain CC, Genet MJ, Detrembleur C, Jérôme C. Chitosan-coated electrospun nanofibers with antibacterial activity. *J Mater Chem B*. 2015;3(17):3508–3517. doi:10.1039/C5TB00158G
88. Wang W, Meng Q, Li Q, et al. Chitosan Derivatives and Their Application in Biomedicine. *Int J Mol Sci*. 2020;21(2). doi:10.3390/ijms21020487
89. Xing J, Zhang M, Liu X, Wang C, Xu N, Xing D. Multi-material electrospinning: from methods to biomedical applications. *Mater Today Bio*. 2023;21:100710. doi:10.1016/j.mtbio.2023.100710
90. Yu H, Li Y, Pan Y, et al. Multifunctional porous poly (L-lactic acid) nanofiber membranes with enhanced anti-inflammation, angiogenesis and antibacterial properties for diabetic wound healing. *J Nanobiotechnol*. 2023;21(1):110. doi:10.1186/s12951-023-01847-w